eNeuro

Research Article: New Research | Development

SAP97 Binding Partner CRIPT Promotes Dendrite Growth *in Vitro* and *in Vivo*

CRIPT mediates the dendritic growth of spinal neurons

Lei Zhang[1], Angela Marie Jablonski[2], Jelena Mojsilovic-Petrovic[1], Hua Ding[3], Steven Seeholzer[3], Ian Paterson Newton[4], Inke Nathke[4], Rachael Neve[5], JinBin Zhai[1], Yuan Shang[6], Mingjie Zhang[6] and Robert Gordon Kalb[1,7]

[1]*Department of Pediatrics Division of Neurology, Research Institute Children's Hospital of Philadelphia, Philadelphia, PA 19104, USA*

[2]*Neuroscience Graduate Group, Department of Neuroscience, University of Pennsylvania, Philadelphia, PA 19104, USA*

[3]*Proteomics Core, Research Institute, Children's Hospital of Philadelphia, Philadelphia, PA 19104, USA*

[4]*Cell & Developmental Biology School of Life Sciences, University of Dundee, Dundee, DD15EH, Scotland*

[5]*Department of Brain and Cognitive Sciences, McGovern Institute for Brain Research at the Massachusetts Institute of Technology, Cambridge, MA 02139, USA*

[6]*Division of Life Science State Key Laboratory of Molecular Neuroscience, Hong Kong University of Science and Technology, Kowloon China Clear Water Bay, Hong Kong*

[7]*Department of Neurology Perelman School of Medicine, University of Pennsylvania, Philadelphia, PA 19104, USA*

DOI: 10.1523/ENEURO.0175-17.2017

Received: 19 May 2017

Revised: 30 October 2017

Accepted: 30 October 2017

Published: 27 November 2017

Author contributions: L.Z., A.M.J., J.M.-P., I.P.N., Y.S., and R.G.K. designed research; L.Z., A.M.J., J.M.-P., H.D., I.P.N., J.Z., Y.S., and R.G.K. performed research; L.Z., A.M.J., S.S., I.S.N., M.Z., and R.G.K. analyzed data; L.Z. and A.M.J. wrote the paper; R.L.N. contributed unpublished reagents/analytic tools.

Funding: http://doi.org/10.13039/100007197HHS | U.S. Public Health Service (USPHS)
NS087077
NS052325

Funding: Program Grant from Cancer Research UK
C430/A11253

Funding: RGC of Hong Kong
AoE-M09-12

The authors declare no competing financial interests.

This work was supported by Public Health Service grants NS087077and NS052325 (R.G.K.) and F31-NS07726 (A.M.J.), as well as program grant C430/A11243 from Cancer Research UK (I.N. and I.P.N.) and grant AoE-M09-12 from the RGC of Hong Kong (M.Z.). We appreciate the gift of the CRIPT plasmids from Maria Passafaro; and PPVD::GFP worms from David Miller. **Some of the *Caenorhabditis elegans* strains were provided by the CGC, which is funded by NIH Office of Research Infrastructure Programs (P40-OD010440). Some strains were also provided by Shohei Mitani (National BioResource Project (NBRP)::*C. elegans*.).**

L.Z. and A.M.J. contributed equally to this work.

Correspondence should be addressed to Robert Gordon Kalb, kalb@email.chop.edu or Robert.Kalb1@northwestern.edu

Cite as: eNeuro 2017; 10.1523/ENEURO.0175-17.2017

Alerts: Sign up at eneuro.org/alerts to receive customized email alerts when the fully formatted version of this article is published.

SAP97 binding partner CRIPT promotes dendrite growth *in vitro* and *in vivo*

Abbreviated Title: CRIPT mediates the dendritic growth of spinal neurons

Lei Zhang[1*], Angela Marie Jablonski[2*],Jelena Mojsilovic-Petrovic[1], Hua Ding[3], Steven Seeholzer[3], Ian Paterson Newton[4], Inke Nathke[4], Rachael Neve[5], JinBin Zhai[1§], Yuan Shang[6], Mingjie Zhang[6], and Robert Gordon Kalb[1,7#]

[1]Department of Pediatrics, Division of Neurology, Research Institute, Children's Hospital of Philadelphia, Philadelphia, PA 19104

[2]Neuroscience Graduate Group, Department of Neuroscience, University of Pennsylvania, Philadelphia, PA 19104

[3]Proteomics Core, Research Institute, Children's Hospital of Philadelphia, Philadelphia, PA 19104

[4]Cell & Developmental Biology, School of Life Sciences, University of Dundee, Dundee, DD15EH

[5]Department of Brain and Cognitive Sciences, McGovern Institute for Brain Research at the Massachusetts Institute of Technology, Cambridge, MA 02139

[6]Division of Life Science, State Key Laboratory of Molecular Neuroscience, Hong Kong University of Science and Technology, Clear Water Bay, Kowloon, Hong Kong, China

[7]Department of Neurology, Perelman School of Medicine, University of Pennsylvania, Philadelphia, PA 19104

*- denotes equal author contribution

§ - Current address, Gene Therapy Program. University of Pennsylvania, 125 S 31st Street, Suite 1300, Philadelphia, PA 191043403

- Current Address, Davee Department of Neurology, Northwestern University Feinberg School of Medicine, 303 East Chicago Avenue, Chicago Illinois 60611-4296

 # Pages: 53

 # Figures: 9

 # Words:

Abstract- 218

Introduction- 425

Discussion- 1,284

Total # Words: 12,997

Supplemental Material: None

Conflict of Interest: The authors declare no competing financial interests.

Corresponding Author email: kalb@email.chop.edu and Robert.Kalb1@northwestern.edu

 # Pages: 52
 # Figures: 8

Abstract- 218
Introduction- 428
Discussion- 1,284

Supplemental Material: None

Conflict of Interest: The authors declare no competing financial interests.

Acknowledgements:

This work was supported by Public Health Service grants NS087077and NS052325 (R.G.K.) and F31-NS07726 (A.M.J.), as well as program grant C430/A11243 from Cancer Research UK (I.N. and I.P.N.) and grant AoE-M09-12 from the RGC of Hong Kong (M.Z.). We appreciate the gift of the CRIPT plasmids from Maria Passafaro; and P_{PVD}::GFP worms from David Miller. Some of the *Caenorhabditis elegans* strains were provided by the CGC, which is funded by NIH Office of Research Infrastructure Programs (P40-OD010440). Some strains were also provided by Shohei Mitani (National BioResource Project (NBRP)::*C. elegans*.) We thank Maria Lim, John Flibotte, and Marco Boccitto for technical assistance and for useful discussion; Yina Dong and David Lynch for the gift of antibodies and plasmids to NR1, NR2A, NR2B, NR2C and NR2D.

ABSTRACT

The dendritic tree is a key determinant of neuronal information processing. In the motor system, the dendritic tree of spinal cord neurons undergoes dramatic remodeling in an activity-dependent manner during early postnatal life. This leads to the proper segmental spinal cord connectivity that subserves normal locomotor behavior. One molecular system driving the establishment of dendrite architecture of mammalian motor neurons relies on AMPA receptors assembled with the GluA1 subunit and this occurs in an NMDA-R- independent manner. The dendrite growth promoting activity of GluA1-containing AMPA receptors depends on its intracellular binding partner, SAP97, and SAP97's PDZ3 domain. We show here that CRIPT is a *bona fide* SAP97 PDZ3-domain binding partner, localizes to synapses with GluA1 and SAP97 along the dendritic tree and is a determinant of the dendritic growth of mammalian spinal cord neurons. We further show that CRIPT has a well-conserved ortholog in the nematode, *Caenorhabditis elegans,* and animals lacking CRIPT display decreased dendrite branching of the well-studied PVD neuron *in vivo*. The lack of CRIPT leads to a selective defect in touch perception and this is rescued by expression of wild type human CRIPT in the nervous system. This work brings new light into the molecular machinery that drives dendritic growth during development and may prove relevant to the promotion of nervous system plasticity following insult.

Significance

Proper dendritic growth is a critical step in the development of neuronal connectivity that underlies proper neuronal communication. Much is known about how NMDA receptors drive neuronal development and plasticity, but less is known about how AMPA receptors contribute in an independent manner. While SAP97 plays a critical role in this process, the molecular mechanisms and binding partners that subserve these effects are under active exploration.

96 Here we show that the cysteine-rich interactor of PDZ3 (CRIPT) is a *bona fide* binding partner of
97 SAP97 in biochemical assays and resides in dendrites in the vicinity of putative AMPAergic
98 synapses. In knockdown experiments, we find that CRIPT is essential for SAP97-dependent
99 dendrite growth *in vitro*. We extend these studies to an *in vivo* model and show that CRIPT is
100 also essential for dendrite growth and mechanosensory function in *C.elegans*. This work links
101 AMPA receptors, MAGUKs and CRIPT to essential neuronal cell biology and *C.elegans*
102 behavior.
103

INTRODUCTION

Activity-dependent development occurs throughout the neuroaxis, including the spinal cord, during early postnatal life (Inglis et al., 2002; Haas et al., 2006; Ni and Martin-Caraballo, 2010). During early postnatal life, motor neurons express a distinct set of excitatory glutamate receptor subunits and this coincides with the period of extensive dendrite growth and remodeling (Jakowec et al., 1995a,b; Stegenga and Kalb, 2001; Jeong et al., 2006). These alterations in dendritic architecture are confined to a critical period and this is subserved by the unique repertoire of glutamate receptors expressed by young spinal cord neurons (Jakowec et al., 1995a,b; Inglis et al., 2002; Jeong et al., 2006).

Activity-dependent growth of the motor neuron dendritic tree is driven by two parallel glutamate receptor mediated processes: 1) an NMDA-R (N-methyl-D-aspartate receptor) – mediated mechanism (Kalb, 1994), and 2) an NMDA-R-independent mechanism (Zhang et al., 2008). This later process depends upon the activation of AMPA-Rs (2-amino-3-(3-hydroxy-5-methyl-isoxazol-4-yl)propanoic acid receptors) assembled with the GluA1 subunit and its intracellular binding partner, synapse associated protein of 97 kDa (SAP97) (Sans et al., 2001; Zhang et al., 2008; Zhou et al., 2008). Animals lacking the GluA1 subunit or SAP97 in motor neurons have a stunted dendritic tree and suffer locomotor impairments that persist throughout life (Zhang et al., 2008; Zhou et al., 2008). All of the dendrite promoting actions of GluA1 are mediated by SAP97 (Zhou et al., 2008). Trafficking of SAP97 to the cell surface is dependent on the interaction with GluA1, but GluA1 trafficks to the cell surface independent of its interaction with SAP97 (Kim et al., 2005; Zhang et al., 2008). SAP97 is a postsynaptic density scaffolding protein with several protein-protein interacting domains organized into the following structure: NH_2 -L27-PDZ1-PDZ2-PDZ3-SH3-U5-GUK-COOH. Recent work indicates that the binding of ligand(s) to the PDZ3 domain of SAP97 is required for SAP97 to promote dendrite growth (Jablonski and Kalb, 2013; Zhang et al., 2015).

To understand the molecular mechanism by which GluA1 and SAP97 promote activity-dependent dendrite growth, we asked: 1) what proteins bind to the PDZ3 domain of SAP97? and 2) what role do such proteins play in dendritogenesis? Here we focus on cysteine-rich-interactor-of-PDZ-three (CRIPT), a 12 kDa protein that localizes to excitatory synapses and links proteins such as postsynaptic-density protein of molecular weight 95 kDa (PSD95) to microtubules (Niethammer et al., 1998; Passafaro et al., 1999). Because PSD95 and SAP97 have a similar domain structure and can functionally complement one another in certain assays (Schlüter et al., 2006; Howard et al., 2010), we asked if CRIPT was a SAP97 PDZ3 ligand and whether it could promote dendrite growth.

MATERIALS AND METHODS

Antibodies

The following antibodies were used in biochemical assays: immunoprecipitation of SAP97 (Thermo Fisher Scientific, catalogue # PA1-741); immunoblotting and immunoprecipitation of CRIPT (Protein Tech Group, catalogue # 11211-1-AP); immunoprecipitation and immunoblotting of HA-tag (BioLegend, 16B11, catalogue # 901512); immunoblotting of SAP97 (NeuroMab/Antibodies Incorporated, catalogue # 73-030); immunoprecipitation and immunoblotting of the myc-tag (Cell Signaling Technology, 9B11 catalogue # 2276); immunoblotting GluA1 (NeuroMab/Antibodies Incorporated, catalogue # 75-327), immunoblotting GluA2 (NeuroMab/Antibodies Incorporated, catalogue # 75-002), immunoblotting GluA4 (Cell Signaling Technology, catalogue # 8070), immunoblotting NR1 (BD pharmingen catalogue # 556308), immunoblotting NR2A (Alomone lab, catalogue # AGC002), immunoblotting NR2B (Alomone lab, catalogue # AGC003),immunoblotting actin (Cell Signaling Technology, catalogue # 3700 (mouse) or Sigma-Aldrich, catalogue # A2066 (rabbit)). The APC antibody used was described previously (Midgley et al, 1997). The following antibodies were used for immunocytochemistry: extracellular epitopes of GluA1 (Alomone, catalogue # AGC004), HA-tag (BioLegend, 16B11,catalogue # 901512 (mouse)), HA-tag (Santa Cruz, Y-11 (rabbit), catalogue # SC-805) and synaptophysin (Sigma-Aldrich, catalogue # SAB4502906)). Secondary antibodies used included for immunocytochemistry: Alexa Fluor 633 or 568 Goat Anti-Mouse IgG (H+L) (Invitrogen) and Alexa Fluor 633 or 568 Goat Anti-Rabbit IgG (H+L) (Invitrogen). When primary antibody was omitted (or pre-immune serum was used), staining with these secondary antibodies yielded no fluorescent signal, thus confirming the specificity of immunocytochemical signal. Secondary antibodies for western blots (IR DYE) comes from Li-COR.

Mixed spinal cultures

Rat mixed spinal cord neuron cultures were prepared as previously described (Jeong et al., 2006; Zhang et al., 2015). They were maintained in glia-conditioned medium supplemented with trophic factors (Alomone Labs at a concentration of 1.0ng/mL): human neurotrophin-3, human neurotrophin-4, human brain-derived neurotrophic factor, human cardiotrophin-1, human glial-derived neurotrophic factor, and rat ciliary neurotrophic factor. One half of the medium was replaced three times per week.

miRNA RNAi design and HSV infection

MiRNA was constructed by annealing two oligomers of 21 base pairs homologous to the CRIPT sequence together and adding BspE1 and FseI restriction sites to the 5' and 3' ends respectively. Annealed oligomers were subsequently cloned into the p1006+ HSV vector using the BspEI and FseI restriction sites. MiRNA was designed against the rat CRIPT sequence corresponding to the ORF: 5'- CTCCACTTGCAGAATTT-3'. We generated an RNAi-resistant CRIPT cDNA containing three silent mutations in the miRNA target sequence of CRIPT by using the QuikChange Site-Directed Mutagenesis Kit using manufacturer's protocol (Agilent). The miRNA target sequence was mutated to: 5'-CTCTACCTGTAGAATTT-3'. Mutated nucleotides are underlined. The p1006+ vector was subsequently used for herpes simplex virus production as previously reported (Neve et al., 1997) . The titer of virus used in these experiments was 3–5 × 10^7 plaque-forming units/mL.

Heterologous cells and transfection

For all experiment except those involving APC, HEK293 cells were maintained in 5% CO_2 at 37°C in Dulbecco's Modified Eagle's medium (DMEM) (Invitrogen) supplemented with 10% fetal bovine serum (FBS) (Sigma), 1% Penicillin/Streptomycin (Pen/Strep) (Sigma). Cells were transfected (Lipofectamine 2000; Invitrogen) per manufacturer's protocol when they were

189 ~75% confluent and were maintained in DMEM with 10% FBS until lysed 48 hours post
190 transfection.

191 For experiments involving APC, HEK293 cells were maintained at 37˚C in 5% CO_2 in
192 DMEM (Life Technologies), supplemented with 10% FBS (GE Healthcare Life Sciences), 1%
193 Pen/Strep (Life Technologies) and nonessential amino acids (1:100; Life Technologies). Cells
194 were transfected using Fugene 6 (Promega), according to the manufacturer's instructions.

195 ***Immunoprecipitation and Western Blotting***

196 For immunoprecipitation experiments not involving APC, lysates were made in 1% NP-
197 40 lysis buffer (25mM Tris-HCl pH 7.4, 150mM NaCl, 1mM EDTA, 1% NP-40, 5% glycerol;
198 150µL per 60mm dish) supplemented with fresh protease and phosphtase inhibitor cocktail
199 (Sigma). After 2 washes in ice-cold 1X phosphate-buffered saline (PBS), cells were lysed in
200 lysis buffer, sonicated (20% strength, 10 seconds), and centrifuged at 13,000xg for 10 minutes
201 (4˚C) to remove cellular debris. 5% of the lysate was saved for input, and the remaining lysate
202 was used for immunoprecipitation. For immunoprecipitation, DynaBeads Protein G (Invitrogen)
203 were pre-cleared in PBS/1% Tween and were bound to the antibodies (4 µg of antibody) (30' at
204 room temperature (RT)). Lysate was added, incubated for 1 hour at RT, and the lysate and
205 bead mixture was washed 3 times in lysis buffer. Proteins were then boiled in 1% BME and 1X
206 SDS loading buffer (40µL total). Proteins were immunoblotted following standard Western
207 blotting technique using 4-12% Bis-Tris gels (Invitrogen) in MES-SDS running buffer
208 (Invitrogen). BioRad SDS-PAGE standards Low Range (Cat # 161-0305) molecular weight
209 markers were used. Gels were transferred onto nitrocellulose (Bio-Rad) at 100V for 1 hour at
210 4˚C and blocked in 5% milk in TBST buffer (50mM Tris-HCl, pH 7.4; 150mM NaCl; 0.1% Tween-
211 20). Primary antibodies were incubated in blocking buffer as indicated overnight at 4˚C.
212 Secondary anti-rabbit and anti-mouse AlexaFluor 800/680-conjugated antibodies (Life

Technologies) were diluted 1:10,000 in 5% milk in TBST buffer and binding was detected using the Odyssey system (LiCor) Infrared Imaging System without saturating the protein bands. The intensity values were normalized against the actin loading control. Quantitative data was the average of no fewer than 3 separate and independent experiments.

For immunoprecipitation experiments involving APC, lysates were made using MEBC lysis buffer (50 mM Tris, pH 7.5, 100 mM NaCl, 5 mM Na-EDTA, 5 mM Na-EGTA, 40 mM β-glycerophosphate, 0.5% NP-40) containing a cocktail of protease inhibitors: leupeptin, pepstatin A, chymostatin (each 10 µg/ml), 1 mM $NaVO_4$, and 10 mM NaF. Cells were scraped and the mixture was spun at 14,000 rpm for 20 min at 4°C. Supernatants were removed and immediately frozen using liquid nitrogen. To measure the binding of endogenous APC to either wild type (WT) or mutant SAP97, 10 µg of polyclonal anti-SAP97 antibody (Fisher Scientific) was pre-bound to 100 µl of 50% protein-A-Sepharose bead slurry (Sigma) by gently agitating the mixture at 4°C for 16 hours. After washing the beads twice with MEBC, 0.5 mg of lysate from cells transfected with WT or mutant SAP97 was added and gently mixed for 16 hours at 4°C. The beads were washed three times with cold MEBC buffer before they were resuspended in 20 µl SDS-PAGE loading buffer and heated to 70°C. Samples (without the beads) were subjected to SDS-PAGE using 4-12% gels (Life Technologies) in MOPS-SDS running buffer (Life Technologies). Proteins were transferred to Amersham Protran nitrocellulose membrane (0.1µm; GE Healthcare Life Sciences). Blots were probed with crude serum from rabbits immunized with N-terminal portion of APC (Midgley et al, 1997) diluted at a concentration of 1:1,000 in blocking solution (Tris-buffered saline, 5% nonfat milk, 1% goat serum and 0.02% Triton X-100) and an anti-SAP97 antibody (Fisher Scientific) diluted 1:1000. Secondary anti-rabbit and anti-mouse AlexaFluor 800/680-conjugated antibodies (Life Technologies) were diluted 1:10,000 and binding was detected with Odyssey (LiCor).

Surface plasmon resonance sample preparation

The PDZ3 domain of SAP97 was amplified by PCR and the PCR product was ligated into the pGEX vector (GE) and transformed into BL21 strain. Correctness of the construct was confirmed by sequencing. GST-PDZ3 fusion protein expression was induced with isopropyl-1-thio-b-D-galactopyranoside (IPTG) for 3 hours. The bacteria were harvested by centrifugation, re-suspended in ice-cold lysis buffer (50 mM Tris, 50 mM NaCl, 5 mM EDTA, 1 µg/ml leupeptin, 1 µg/ml pepstatin, 0.15 mM PMSF, 1 mM 2-mercaptoethanol), and lysed by sonication on ice. The bacterial lysates were cleared by centrifugation, and supernatant was collected and incubated with glutathione Sepharose 4B matrix. After extensive washes with lysis buffer, glutathione Sepharose 4B resin was incubated with freshly made 10 mM glutathione buffer (50 mM Tris, 10 mM reduced glutathione, pH 8.0) to elute the GST fusion protein. Purified GST-PDZ3 fusion protein was further dialyzed to remove glutathione before plasmon resonance studies.

Surface plasmon resonance (SPR) measurements and affinity analysis of sensorgrams.

Association and dissociations reactions of peptides CHRK1 (C-terminal amino acids of CRIPT) or CHRK2 (C-terminal amino acids of CRIPT V101A) (as analytes) and recombinant GST fusion protein GST-PDZ3 and GST (as ligands) were performed using a Biacore3000 instrument. Anti-GST antibody was immobilized on flow cell 3 and 4 according to the manufacturer's instructions. GST and GST-PDZ3 were then captured on flow cell 3 and flow cell 4 separately, where GST served for on-line reference subtraction (values shown in data subtract any signal from this negative control). Both the analytes and the ligands were dissolved in the HBS running buffer (0.01M Hepes, 0.15M NaCl, 3mM EDTA, 0.005% v/v Surfactant P20) and their concentrations were determined at UV280nm using extinction coefficients calculated from the amino acid composition. The ligands were bound as densities between 1200RU and 1700RU. The analytes of CHRK1 and CHRK2 in 45uL volume each with various concentrations

(62.5nM, 250nM, 4μM, 8μM, 10.24μM and 12.8μM) were injected over both GST and GST-PDZ3 surfaces at flow rate of 30μL/min. Dissociation time was monitored for 3min. A 40 second pulse of glycine-HCl pH2.2 was applied to regenerate the GST surface. For GST-PDZ3 surface regeneration, an additional 40 s pulse of glycine-HCl was applied. Analysis of steady-state affinity was performed using BIAevaluation software selecting reference-subtracted curves with a 1:1 interaction model. Affinity constant K_d was derived from Req vs. C (response unit at equilibrium vs. peptide concentration) plot with the steady-state affinity model fit. Data for GST capture was subtracted from GST-PDZ3 values.

Neuronal transfection and neuron tracings

At 5 days *in vitro* (DIV), mixed spinal cultures were transfected (Lipofectamine 2000; Invitrogen) with the overexpression plasmid or microRNA (miRNA) being tested in a 3:1 ratio with GFP to ensure all GFP-positive cells also expressed the desired construct. 5 days after transfection, cells were fixed in 4% paraformaldehyde (PFA) and immunostained with rabbit anti GFP antibody and secondary antibody. After immunostaining, the coverslip with the cells was mounted on the slide and viewed using fluorescent microscopy. Neuronal tracings were performed with the Neurolucida program (MicroBrightField) and analyzed with the Neuroexplorer program (MicroBrightField). As previously described (Zhang et al., 2008), the minimum inclusion criteria for this study were: dendrites radially distributed (>180°) and no more than one primary dendrite is truncated (less than three times the cell body diameter). In addition, only processes ≥ 4μm were included in our analysis since this distinguishes true branches from dendritic filopodia (Zhang et al., 2015). Quantitative descriptors of the dendrites were as follows (Zhang et al., 2015): “1° dendrites,” the number of primary dendrites leaving the cell body, “branches, #”, the number of dendritic bifurcations, “Σlength”, sum of the linear length of all dendrites from a single cell, “average dendrite” = the sum of the lengths of all dendritic shafts from a single neuron divided by the number of primary dendrites and “longest dendrite,” the

length of the longest dendrite from the cell body to the most distal tip. Spinal cord cultures were created over a 6-year period for these experiments and all the anatomical drawings were performed by a single operator (L. Zhang) blinded to experimental group. All drawings of neurons within a specific experiment (i.e. three groups in Figure 4, panel B; Figure 4, panel C; etc) were done contemporaneously. Since specific experiments were performed over 6 years, absolute values obtained for one specific experiment can not be directly compared with the absolute values obtained for a second specific experiment. Sources of variation include differences in batches of serum, Dams from different venders, etc.

Immunocytochemical localization of CRIPT in mixed spinal cord cultures

We found none of the commercially available antibodies to CRIPT or SAP97 were suitable for immunocytochemical studies (e.g., Abcam; ProteinTech Group; Santa Cruz Biotechnology, NeuroMab). We devised an alternative strategy for visualizing CRIPT in neurons. We co-transfected neurons with a miRNA designed to knockdown endogenous CRIPT alongside an RNAi-resistant version of WT CRIPT containing a hemagglutinin (HA) tag on the amino terminus. When these plasmids were co-transfected with a GFP reporter and stained for HA, we visualized punctate HA immunoreactivity in the cell body and dendrites of transfected neurons. The molar ratio of the transfected plasmids (e.g., GFP : CRIPTmiRNA : RNAi resistant HA-CRIPT was 1 : 5 : 2) to ensure that HA staining was restricted to neurons with a high likelihood of concomitant knockdown of endogenous CRIPT. Both mouse anti-HA (BioLegend) and rabbit anti-HA (Santa Cruz Biotechnology) worked well in this application. In one set of experiments, we used a mammalian expression vector engineered to express GFP-SAP97 in localization studies.

Membrane protein preparations

Cells were washed twice using ice-cold PBS and suspended in hypotonic lysis buffer (10 mM KCl, 1.5 mM $MgCl_2$, and 10 mM Tris-Cl, pH 7.4; 1.5 mL/60 mm plate). After incubation on ice for 10 minutes, cell lysis was finalized using a homogenizer (Dounce). The cell lysate was centrifuged at 2000 × g for 2 min (4°C) to remove nuclei and cellular debris and the supernatant was centrifuged a second time at 100,000 × g for 30 min at 4°C to pellet cell membranes. The supernatant was saved as the 'cytoplasmic' fraction and the pellet ('membrane' fraction) was resuspended in RIPA buffer (50mM Tris-HCl pH 7.5, 150mM NaCl, 1mM EDTA, 1mM EGTA, 1% NP-40, 1% sodium deoxycholate) supplemented fresh with protease and phosphatase inhibitor cocktail (Sigma). Lysates were boiled for 5 minutes in 1% BME (Bio-Rad) and 1X SDS-loading buffer prior to standard western blotting technique as described earlier using 4-12% Bis-Tris gels (Invitrogen) in MES-SDS buffer (Invitrogen).

Yeast-two-hybrid

The PDZ3 domain of SAP97 flanked by 5 amino acids on the amino- and carboxy-termini was amplified by PCR and cloned into the yeast bait phagemid pBD-GAL4. Full-length CRIPT was engineered into the yeast prey phagemid pAD-UAS. YRG-2 yeast were transformed (Clontech) according to the manufacturer's instructions with phagemids or appropriate empty vector controls and grown under restrictive conditions (SD media lacking leucine, tryptophan, and/or histidine) and single colonies were subsequently streaked onto restrictive plates. The plasmid, pGBT9, was used as a positive control.

CRIPT and SAP97 structural modeling

The SAP97 PDZ3 model was built in SWISS-MODEL on-line server (http://swissmodel.expasy.org/). PSD95 PDZ3/CRIPT (PDB id:1BE9) was selected as the template in the modeling process. For the SAP97/PDZ3/CRIPT complex, CRIPT peptide was modeled from PSD95 PDZ3/CRIPT complex (PDB id:1BE9).Then, both the complex structure was further adjusted manually to take the N-terminal upstream residues of CRIPT into account. Finally, the structure model was submitted to YASARA Energy Minimization server

(http://www.yasara.org/minimizationserver.htm) to achieve the final SAP97/CRIPT complex model.

C. elegans maintenance

All *C. elegans* strains were maintained using standard methodology (Brenner, 1974). Animals were maintained at 20˚C on nematode growth medium (NGM) agar plates with live OP50 bacteria. A worm strain containing a deletion within the *C. elegans* ortholog of CRIPT, *tm430*, was obtained from National BioResource Project in Japan and backcrossed three generations to ancestral N2 before being crossed into the P_{PVD}::GFP line. We also utilized the *mec-4* (*u253*) and *mec-3 (e1338)* strains which were obtained from the Caenorhabditis Genetics Center (CGC). The *mec-4* (*u253*) strain was backcrossed 3 generations to ancestral N2 before being analyzed and crossed into the *tm430* strain.

C. elegans rescue cloning and lines

Human CRIPT (hCRIPT) cDNA was amplified using PCR. Gateway cloning (Invitrogen) was employed and the BP reaction was used to construct the pDonR221-hCRIPT (pEntry:: hCRIPT) construct. The LR reaction was then performed using the following constructs for the 1^{st}, 2^{nd}, and 3^{rd} positions respectively: unc-119 promoter, pEntry::hCRIPT, and the unc-54 3'UTR. The LR reaction was performed to insert this cassette into the pCFJ150 destination plasmid for *C. elegans* expression. Sanger sequencing was used to confirm the correctness of the final construct, $P_{unc-119}$::hCRIPT::unc-54 3'UTR (P_{neuron}::hCRIPT) enabling the expression of hCRIPT in the *C. elegans* nervous system. To create transgenic extrachromasomal arrays, P_{neuron}::hCRIPT was injected into the gonads of the indicated strains (at one day post the fourth larval stage ("L4")) at a final concentration of 50ng/μL along with a co-injection marker, pCFJ150 (P_{myo-2}::mCherry) at a final concentration of 5ng/μL. The final DNA concentration of the injection mix was 100ng/μL; a sonicated LacZ plasmid was used to arrive at the proper final DNA

concentration as needed. At least 3 independent transgenic lines were created for each final strain and all were tested in corresponding assays.

C. elegans imaging

All lines were synchronized before visualizing GFP-labeled PVD neurons. Briefly, young adult (1 day post L4) hermaphrodites were allowed to lay eggs for 4-6 hours. At the L4 stage, noted by the presence of a clear vulva, animals were moved to a separate plate and imaged one day later. Animals were immobilized using levamisole (10mM; Sigma) on fresh 4% agar pads and imaged using confocal microscopy. Z-stacks were obtained and merged, and was analyzed by manually counting the number of dendrites present on the PVD neuron dendritic tree (Smith et al., 2010, 2013) from the cell body to the posterior end of the animal. The number of primary, secondary, and tertiary dendrites was determined as previously described (Liu and Shen, 2011). The analyst was blind to experimental group during image acquisition and analysis.

C. elegans touch assay

In the touch assay, the midsection of the body near the vulva was gently prodded with a platinum wire, as previously described (Way and Chalfie, 1989). A positive response was scored as movements of at least one body length in response to the touch stimulus, although the speed of the animal can vary in different mutant backgrounds.

Statistics

Statistical analysis was performed using GraphPad Prism Version 6.00 for Windows, GraphPad Software, La Jolla, CA, USA (www.graphpad.com). Unpaired t-test was used for all two-group comparisons. For data more than three groups, a one-way ANOVA with Dunnett's multiple comparisons test was used. For analysis of the neuronal tracings, a Shapiro–Wilk test

was run to test normality of the data (SPSS). If the data were normally distributed, the data were analyzed with one-way ANOVA. Post-hoc analysis was performed with Tukey test. If the data did not distribute normally, a non-parametric Kruskal-Wallis H test (e.g., one way ANOVA on ranks) was used to analyze data. Post-hoc analysis was performed with Dunnett's test. The threshold for significance was set at $p < 0.05$ for all tests. Data is presented as mean ± standard error of the mean.

RESULTS

CRIPT interacts with SAP97's PDZ3 domain

Recent work has revealed that the third PDZ domain of SAP97 is critical for the pro-dendrite-growth activity of SAP97 (Zhang et al., 2015). Identification of the endogenous SAP97 PDZ3 domain ligand(s) responsible for this biological activity is problematic because the list of candidates contains ~90 potential binding partners (see "interactions" at http://www.ncbi.nlm.nih.gov/gene/25252). In an attempt to focus the search, we noted that there is 86% sequence homology between the PDZ3 domain of SAP97 and the PDZ3 domain of PSD95 (Figure 1A). Since CRIPT binds to the PDZ3 domain of PSD95 (Niethammer et al., 1998), we tested CRIPT binding to the PDZ3 domain of SAP97. We used a heterologous expression system in HEK293 cells and established that full-length (FL) hemagglutinin (HA)-tagged CRIPT (HA-CRIPT) and FL myc-tagged SAP97 (myc-SAP97) co-immunoprecipitated (Figure 1B). Anti-HA IgG, but not a control IgG, successfully co-immunoprecipitates HA-CRIPT and myc-SAP97. To determine if the PDZ3 domain of SAP97 mediates this interaction, we attempted to co-immunoprecipitate HA-CRIPT with versions of FL SAP97 containing ligand-binding-disabling mutations in either the PDZ2 (K323A, K326A) or PDZ3 (H469A, R470A) domain. We found that mutations in the PDZ3 domain, but not in the PDZ2 domain, completely abolished binding of CRIPT to SAP97 (Figure 1C). Next, we attempted to co-immunoprecipitate FL myc-SAP97 with two versions of CRIPT: 1) a wild type (WT) FL CRIPT and (2) a version of FL CRIPT harboring a point mutation in the C-terminal valine (the PDZ3 binding motif of CRIPT, -QTSV). This mutation was previously shown to disrupt the binding of CRIPT to PSD95 (referred to as CRIPT V101A), but not CRIPT's binding to microtubules (Passafaro et al., 1999). We found that the V101A mutation prevented CRIPT's binding to SAP97 (Figure 1D). As a specificity control, we asked if another SAP97 binding partner, adenomatous polyposis coli (APC), also showed differential binding. In contrast to CRIPT, APC was pulled down

equivalently by WT SAP97 and PDZ3 mutant SAP97 (Figure 1E). Taken together, these data suggest that CRIPT specifically interacts with the third PDZ domain of SAP97 and this interaction relies on the canonical PDZ-interaction motif of CRIPT at its C-terminus.

We complemented these observations with two further approaches. First, in a yeast-two-hybrid (Y2H) assay, we found that full-length CRIPT interacts with the PDZ3 domain of SAP97. FL CRIPT neither interacted with an empty bait vector, nor did the SAP97 PDZ3 domain interact with an empty prey vector (Figure 1F). Second, surface plasmon resonance (SPR) studies were performed with immobilized GST-PDZ3 or GST and peptides corresponding to the C-terminal 18 amino acids of CRIPT. We found that WT CRIPT peptide bound to the PDZ3 domain of SAP97 with a K_d of 6.57μM, while V101A mutant showed no saturable binding to the PDZ3 domain of SAP97 (Figure 1G). Prior work suggests that ligand binding to PDZ domains can vary substantially as a function of: 1) method (i.e. SPR or fluorescence polarization) (Hung and Sheng, 2002) and 2) the length, in amino acids, of the peptide ligand (i.e. longer peptides displaying lower K_d). Niethammer et al. showed that a peptide corresponding to the C-terminal 9 amino acids of CRIPT binds to the PSD95 PDZ3 with a K_d = ~ 1μM (Niethammer et al., 1998). These results can not be directly compared with our observations because Niethammer et al used fluorescence polarization as opposed to SPR. Nonetheless our observations are within the range of reported affinities for ligand binding to isolated PDZ3 (Irie et al., 1997) and as such are consistent with a direct interaction between the PDZ3 domain of SAP97 and the C-terminus of CRIPT.

To study a more physiological setting, we asked if CRIPT and SAP97 co-immunoprecipitated using lysates prepared from mixed spinal cord cultures. Anti-CRIPT antibody, but not a control IgG, was able to immunoprecipitate CRIPT and SAP97 together (Figure 1H). Immunoreactivity at ~50 kDa and ~25 kDa in the “input” lane may represent a minor amount of spill over from the adjacent “control IgG” lane. As expected, prominent

immunoglobulin heavy and light chain bands are present in the immunoprecipitated material, as seen in the control IgG and the anti-CRIPT IgG lanes. This experiment confirms that endogenous CRIPT and SAP97 physically interact within a nervous system setting.

The above described biochemical studies make the case for a direct physical interaction between CRIPT and PDZ3 of SAP97. However, all biochemical studies come with caveats and it remains possible that the interaction between CRIPT and PDZ3 of SAP97 (Figure 1 panels B – H) is indirect. To gain further insight into this potential binding, we attempted to model this interaction at the atomic level. We began by refining the deposited PSD95 PDZ3/CRIPT interaction and then modeled the SAP97 PDZ3/CRIPT complex based on the refined PSD-interacting features (Figure 2). The main residues directly involved in CRIPT binding to PDZ3 of PSD95 and SAP97 are conserved (highlighted in yellow in Figure 1A). The C-terminal three residues of CRIPT that bind to PDZ3 of PSD95 and SAP97 are identical. In the PSD95/CRIPT structure, the side chains of D332 in PSD95 and K(-4) in CRIPT are not defined in the original crystal structure. In our modeled structure, K(-4) of CRIPT forms a salt-bridge with D332 of SAP97 PDZ3. Additionally, K(-7) of CRIPT forms a pair of salt-bridges with D485 and E487 from the beta strand B/alpha helix C (βB/αC-loop) of SAP97 PDZ3. Finally, Y(-5) of CRIPT interacts with the hydrophobic residues in the C-terminal α-helix extension of SAP97. These additional charge-charge, hydrogen bonding, and hydrophobic interactions between the N-terminal sequences of the CRIPT peptide and the αB/αC-loop of PDZ3, in addition to the canonical PDZ binding motif and PDZ3 interactions, could enhance both the binding affinity and specificity between SAP97 and CRIPT. This new *in silico* analysis provides a plausible physical means by which CRIPT could directly interact with SAP97.

Previous localization work (at the light and electron microscopic levels) places CRIPT in the postsynaptic density approximately 35 nm from the inner leaflet of the plasma membrane and hippocampal cultures, CRIPT co-localizes with PSD95 at excitatory synapses(Niethammer et al., 1998). In light of the known physical interaction between GluA1 and SAP97 (Sans et al., 2001; Zhou et al., 2008; Zhang et al., 2015) we explored the localization of these proteins and their relationship to synapses using immunocytochemical tools in mixed spinal cord cultures. The antisera generated to CRIPT by the Sheng lab (Niethammer et al., 1998) is no longer available and despite investigating a variety of fixation protocols, we found that none of the commercially available antibodies to CRIPT were suitable for immunocytochemical imaging of endogenous CRIPT. To overcome this difficulty, we knocked down endogenous CRIPT and co-expressed an RNAi resistant HA-tagged CRIPT (see Experimental Procedures). CRIPT immunoreactivity was seen in the cell soma and throughout the dendritic tree (Figure 3 and 4), as previously reported by Niethammer et al.(Niethammer et al., 1998); axons appear devoid of CRIPT immunoreactivity. This pattern of immunoreactivity is very similar to that described by Niethammer et al. (Niethammer et al., 1998) (see Figure 5, panels B, E and G).

Niethammer et al. describe CRIPT localization to synapses on dendritic spines (Niethammer et al., 1998). In our spinal cord neuron cultures we do not typically see dendritic spines (Zhang et al., 2015) yet we find that CRIPT is juxtaposed to (and partially overlaps with) synaptophysin puncta on the shafts of dendrites (Figure 3). Niethammer et al. describe the localization of CRIPT with PSD95 (Niethammer et al., 1998) and we too find that CRIPT is juxtaposed to (and partially overlaps with) SAP97 as well as GluA1 (Figure 4).

It is important to note, however that the focal accumulations of CRIPT that we describe here (Figure 3 and 4) and their partial co-localization with SAP97 and GluA exist within a background of diffuse CRIPT immunoreactivity within dendrites. We can not rule out the possibility that some of the immunocytochemical signal is a result of the knockdown and

replacement strategy we employ and thus only approximates the distribution of the native protein *in situ*. Given these caveats, our results suggest that a portion of dendritic shaft CRIPT apparently localizes to synapses along with components of AMPA receptor complexes such as GluA1 and SAP97. This would be consistent with the immunogold electron microscopic localization studies of Niethammer et al. (Niethammer et al., 1998). The precise relationship between these complexes and those defined by Niethammer et al. (Niethammer et al., 1998) (e.g., composed of GRIN2B, PSD95 and CRIPT) will require further inquiry. Super-resolution microscopy, array tomography (Micheva et al., 2010) and the proximity ligation *in situ* assay (Söderberg et al., 2006) are imaging technologizes particularly well suited for inquiry into the fundamental relationship between these proteins.

CRIPT is necessary for proper dendrite growth

To identify the functions of CRIPT, we began by using RNA interference (RNAi) to knockdown CRIPT in mixed spinal cord cultures. We targeted a microRNA (miRNA) to the rat ortholog of CRIPT, engineered it into a Herpes Simplex Virus (HSV) amplicon vector, and infected DIV14 mixed spinal cord cultures with the virus and probed for CRIPT. We determined that the CRIPT miRNA, but not a miRNA to a scrambled sequence (control), effectively knocked down CRIPT in neurons *in vitro* (Figure 5A). Using this tool, we knocked down CRIPT in spinal cord neurons and quantitatively analyzed dendritic architecture. To do this, we compared the dendritic tree of three experimental groups: 1) GFP alone, 2) GFP + the scrambled miRNA and 3) GFP + active CRIPT miRNA by making camera lucida drawings of the dendritic trees in each condition. To assess the effect of CRIPT knockdown on dendritic morphology, we characterized a number of architectural features as described in Experimental Procedures (Zhang et al., 2008; Zhou et al., 2008; Zhang et al., 2015). Group differences were found in branch number (Kruskal-Wallis H test, $H_{(2,73)} = 14.152$, $p = 0.001$) and total dendrite size (ANOVA, $F_{(2,73)} = 6.893$, $p = 0.002$). We found that knockdown of CRIPT led to a ~30% reduction in the number

of dendritic branch points compared to GFP alone ($p < 0.05$) or scrambled miRNA ($p < 0.01$) treated neurons (Figure 5B). In addition, we found that knockdown of CRIPT also led to a ~20% decrease in the total size of the dendritic tree compared to GFP alone ($p < 0.0002$) or the scrambled miRNA ($p < 0.05$). To confirm the effect of CRIPT knockdown was in fact due to the reduced levels of CRIPT, we created an RNAi-resistant CRIPT cDNA ($CRIPT^{res}$) by introducing silent mutations into the CRIPT miRNA target sequence (see Experimental Procedures). We confirmed that $CRIPT^{res}$ was resistant to knockdown by the CRIPT miRNA, compared to the wild type version of CRIPT ($CRIPT^{wt}$) when expressed in HEK293 cells (Figure 5C). With this tool at our disposal, we compared the dendritic architecture of 3 experimental groups: 1) GFP + scrambled miRNA; 2) GFP + CRIPT miRNA; 3) GFP+ CRIPT miRNA + $CRIPT^{res}$. Group differences were seen in branch number ($H_{(2,73)} = 9.846$, $p = 0.007$) and total dendrite size ($H_{(2,73)} = 9.364$, $p = 0.009$). CRIPT knockdown again reduced the total number of branches ($p < 0.05$), as well as the total size ($p < 0.01$), of the dendritic tree compared to the scrambled miRNA (Figure 5D). Rescuing CRIPT expression in CRIPT knockdown neurons using the $CRIPT^{res}$ cDNA completely reversed this effect. There was no difference in any of the dendritic parameters tested compared to the scrambled miRNA (Figure 5D). These data suggest that CRIPT is required for proper dendritic growth *in vitro* in mammalian spinal cord neurons.

CRIPT is not sufficient to induce growth of the dendritic tree

We next asked if increasing CRIPT expression influenced dendrite architecture. At the outset, we considered the possibility that only a limited number of CRIPT binding sites exist at the plasma membrane. This would potentially mask a dendrite growth promoting phenotype of CRIPT overexpression. To test this idea, we overexpressed two different versions of CRIPT in spinal cord neurons: 1) WT CRIPT and 2) a version of CRIPT that was palmitoylated at the N-terminus of CRIPT to allow CRIPT to traffic to the cell surface (pal-myc-CRIPT). The palmitoylation sequence was derived from paralemmin-1 and placed on the N-terminus of

CRIPT. Subcellular fractionation followed by Western blot confirmed that palmitoylated CRIPT (pal-myc-CRIPT) is found predominantly in the membrane fraction, whereas CRIPT without the palmitoylation sequence is predominantly cytosolic in this preparation (Figure 5E). To determine if overexpression of these CRIPT constructs influenced dendritic architecture, we compared 3 groups: 1) +GFP; 2) +WT CRIPT; and 3) +pal-myc-CRIPT. By Kruskal-Wallis H test, no group differences were found (Figure 5F). Taken together, these overexpression studies indicate that CRIPT alone is not sufficient to promote dendrite growth on its own, even when CRIPT is artificially targeted to the plasma membrane to overcome any potential saturation of CRIPT membrane-binding sites.

CRIPT is required for the dendrite growth promoting activity of SAP97

Prior work has shown that SAP97 promotes dendritic growth of motor neurons *in vitro* and *in vivo* (Zhang et al., 2008; Zhou et al., 2008). We next asked if CRIPT was required for the dendritic growth promoting activity of SAP97. To address this question, three groups of neurons were studied: 1) +GFP; 2) +SAP97 + scrambled miRNA; and 3) SAP97 + CRIPT miRNA. Group differences were seen in branch number ($H_{(2,73)}$ = 8.212, p = 0.016) and total dendrite size ($H_{(2,73)}$ = 8.592, p = 0.014) . In the presence of the scrambled miRNA, overexpression of SAP97 led to a ~30% increase in the total length and ~30% increase in branch number of the dendritic tree compared to transfection with GFP alone ($p < 0.05$) (Figure 6) consistent with past findings (Zhang et al., 2008). The promotion of dendritic growth by overexpression of SAP97 was entirely blocked when CRIPT was knocked down in the same group of neurons (Figure 6). These observations suggest that CRIPT is required for the dendrite growth-promoting actions of SAP97 and is part of the machinery required for SAP97-dependent developmental phenotypes.

Loss of CRIPT influences the expression of select components of excitatory synapses

Passafaro et al. reported that CRIPT influences postsynaptic MAGUK clustering without affecting NMDA receptors or synaptophysin-labeled presynaptic elements (Passafaro et al., 1999). These observations and conclusions were based on use of a cell-penetrating peptide (16 amino acids of the antennapedia homeodomain) linked to the C-terminal 9 amino acids of CRIPT ("antp-CRIPT"). While antp-CRIPT had the virtue of competing (and therefore blocking) the interaction all proteins that bind to the C-terminus of CRIPT, this reagent also act as a dominant-negative inhibitor of ligands for PDZ3 of all MAGUKs. Thus the specific role of CRIPT in synaptic molecular biology is undefined. To begin to address this issue, we knocked down CRIPT in spinal cord cultures using the validated miRNA described above and prepared lysates for Western blots. We find that knock down of CRIPT led to a significant reduction in the abundance of GluA1 and SAP97, but had no effect on the abundance of GluA2, GluA4, NR1, NR2A, NR2B or PSD95 (Figure 7). Thus loss of CRIPT leads to very specific changes in components of AMPA receptors and PSD MAGUKs. These observations are the first clues suggesting that CRIPT can regulate excitatory neurotransmission (through changes in hetero-oligomeric assembly of AMPA receptors) and downstream consequences (through changes in the composition of the postsynaptic density). The use of dynamic reporters of synaptic function, electrophysiology and super-resolution microscopy will be required in the future to precisely define the molecular mechanisms of CRIPT action on synaptic biology.

CRIPT promotes dendritic growth in vivo

Our understanding of *in vivo* biology of CRIPT is hampered by the fact that CRIPT null mice die at E9 and no conditional alleles exist. One potential path forward is to study the *in vivo* effects of CRIPT in phylogenetically lower animals. CRIPT is an ancient gene and was likely to exist in the last common ancestor prior to the split of the Animalia and Plantae kingdoms of life. The *C.elegans* genome contains a CRIPT ortholog (C36B1.14) that is 38.8% identical to human CRIPT and both proteins are very basic (pI human CRIPT is 9.57 and pI of *C.elegans* CRIPT is

586 9.61). CRIPT message is expressed in embryonic (Stetina et al., 2007; Moore et al., 2005),
587 early larval (Stetina et al., 2007) and adult (Kaletsky et al., 2016) neurons (and see
588 http://www.vanderbilt.edu/wormdoc/wormmap/WormViz.html). The cardinal feature of human
589 CRIPT is 8 cysteine residues and *C.elegans* CRIPT has 7 cysteine residues in register with their
590 locations in the human protein. A mutant allele of *cript* allele exists (*tm430* contains a ~400bp
591 deletions near the C-terminal region of the protein, which would eliminate CRIPT's PDZ-
592 interaction motif) and is likely to be a null. In light of these considerations, we studied of the *in*
593 *vivo* biology of CRIPT biology in *C.elegans.*

594 We began by asking if loss of CRIPT influences the size and complexity of the dendritic
595 tree of a single neuron. To this end, we used a *C. elegans* reporter strain with GFP expressed
596 in the well-characterized PVD mechanosensory neuron (Smith et al., 2010; Smith et al., 2013).
597 The PVD neuron dendrites showed an ~25% decrease in the branches of secondary and
598 tertiary dendrites in the *cript(tm430)* background versus the wild type (N2 Bristol strain)
599 background (*$p < 0.05$) (Figure 8A-D). We next asked if the dendrite growth defect of the *cript*
600 mutant was due to the loss of expression of CRIPT in neurons. To study this, we expressed
601 human CRIPT under the control of a nervous system specific promoter ($P_{unc-119}$::hCRIPT)
602 ('P_{neuron}::hCRIPT') in *cript* (*tm430*) mutants with GFP labeled PVD neurons. We found that
603 neuronal expression of human CRIPT was sufficient to rescue the decrease in secondary and
604 tertiary branches in the *cript* (*tm430*) mutant to wild type levels (Figure 8D). This effect was seen
605 in three independently generated transgenic lines (data not shown). Although we have no direct
606 evidence that CRIPT is expressed at physiologically relevant levels in PVD neurons, the fact
607 that pan-neuronal expression of hCRIPT rescues the abnormalities in the PVD neurons
608 dendrites in the *cript(tm430)* background, enables two observations: 1) the loss of neuronal
609 CRIPT is responsible for the dendrite phenotype of PVD neurons in the *cript(tm430)* animals,
610 and 2) while parsimonious to infer that changes in CRIPT within PVD neurons themselves
611 account for these observations, our results are equally consistent with the idea that CRIPT has

non cell-autonomous effects on neuronal biology in the worm. In this later scenario, CRIPT expression in non-PVD neurons might influence network activity, for example, and thereby influence PVD neurons. It is also worth remembering that PVD neurons are sensory and the extent to which they are activated by glutamate receptors (as with our studies of mammalian neurons *in vitro*) is an open question. Regardless of these specific details, our observations are the first *in vivo* demonstration that CRIPT is essential for normal dendrite elaboration and illustrate the remarkable evolutionary conservation CRIPT function.

Loss of cript causes a mechanosensory defect in vivo

We wondered if the anatomical defects in PVD neuron dendrites incurred by loss of *cript* had functional consequences. *C. elegans* response to gentle stroking by an eyelash is mediated by six neurons: ALML/R (where "L" and "R" refer to the left and right side of the body), PLML/R, AVM and PVM (Chalfie and Sulston, 1981). This "light touch" response is lost in animals with mutation in the amiloride-sensitive sodium channel encoded by the *mec-4* gene. However, animals with mutation in *mec-4* do respond to a stronger mechanical stimulus (e.g., touching the midsection of the animal with a platinum wire) and this response is lost when the PVD neuron is eliminated by laser ablation (Way and Chalfie, 1989). The "harsh touch" response is mediated by ALML/R, PLML/R, PVD and perhaps the FLP sensory neurons. PVD function is typically assayed in a *mec-4* mutant background as this eliminates the light touch response and thus isolates PVD-dependent behaviors (Liu and Shen, 2011). As a positive control in touch assays, investigators use *mec*-3(*e1338*) animals because they are insensitive to both light and harsh touch (Way and Chalfie, 1989; Liu and Shen, 2012). We took advantage of this simple yet powerful system to inquire if the reduced branching of the dendritic arbors of the PVD neuron seen in *cript* mutants was associated with a functional deficit in the harsh touch assay. We compared the response to harsh touch in 5 *C. elegans* strains: 1) the wild type N2 (a negative control); 2) *mec-3(e1338)*; 3) *cript* (*tm430*); 4) *mec-4*(*u253*); and 5) *cript* (*tm430*); *mec-*

637 *4* (*u253*) double mutants (Figure 8 E). By ANOVA, group differences were found ($F_{(4,10)}$=11.93;
638 p = 0.0008). Using post-hoc analysis, we confirmed that ~40% of *mec-3(e1338)* mutant animals
639 were defective to harsh touch (p < 0.05) (they did not respond or move in response to stimulus)
640 in comparison to wild type animals, in which only 10% displayed a lack of response to harsh
641 touch. The *cript* (*tm430*);*mec-4* (*u253*) double animals displayed a significant (p < 0.01) defect
642 to harsh touch in ~50% of animals compared to wild type animals. There were no significant
643 differences between the single mutants (i.e. *cript* (*tm430*) or *mec-4* (*u253*)) and N2 worms
644 (Figure 8 E). These observations indicate that the *cript* mutants are incapable of compensating
645 for the loss of *mec-4*. This functional impairment could be due to the observed abnormality in
646 dendrite growth of *cript* mutants.

647 Finally, we asked if expression of hCRIPT in the nervous system of *cript* mutant (*tm430*)
648 worm would restore harsh touch sensitivity in the *cript* (*tm430*);*mec-4* (*u253*) animals. We found
649 that expression of human CRIPT in the nervous system (P_{neuron}::hCRIPT) was sufficient to
650 partially rescue the harsh touch defect of the *cript* (*tm430*);*mec-4* (*u253*) animals. Approximately
651 ~55% percent of *cript* (*tm430*);*mec-4* (*u253*) animals showed a harsh touch defect and this was
652 reduced to ~25% when hCRIPT was expressed in the nervous system (p < 0.01). This effect
653 was found in 4 independently generated transgenic lines (Figure 8 F). These observations
654 suggest that neuronal CRIPT is required for normal touch responses in *mec-4*(*u253*) mutant
655 animals. Although pan neuronal expression of hCRIPT both rescues the PVD neuron dendrite
656 abnormality and touch sensitivity *cript* (*tm430*); *mec-4* (*u253*) animals, our data do not
657 distinguish between a cell autonomous versus cell non-autonomous role of CRIPT. It remains
658 possible that CRIPT expression in neurons, in addition to the touch critical neurons such as
659 PVD underlie, these observations.

DISCUSSION

SAP97 is a modular scaffolding protein that localizes to the postsynaptic density and plays an essential role in translating the activity of AMPA-R assembled with GluA1 into appropriate dendrite growth and ensuring proper circuit patterning (Zhang et al., 2008; 2015). We show here that CRIPT is a *bona fide* binding partner of the pro-dendrite growth domain of SAP97, PDZ3. Our observations provide novel insights into the currently limited knowledge about CRIPT biology by showing that CRIPT is required for normal dendrite growth both *in vitro* and *in vivo*. In addition, we show that the loss of CRIPT in neurons causes behavioral defects, highlighting the functional importance of CRIPT in organizing neuronal circuits. The relevance of our results is suggested by the identification of children with mutations in CRIPT. Two children with homozygous, likely null, mutations are microcephalic and severely encephalopathic (Shaheen et al., 2014); another child with a compound heterozygous mutation is also microcephalic and displays global developmental delay (Leduc et al. 2016) Thus, while MAGUKs such as PSD95 and SAP97 can substitute for each other in electrophysiological assays (Schluter et al., 2006; Howard et al., 2010), our data indicate that CRIPT has a non-redundant and critical cell biological function in neurons.

Many factors influence the computational work of neurons including: 1) the size, geometry and complexity of the dendritic tree (Stuart, 1999), 2) the quantitative and qualitative nature of the afferent input (Hume and Purves, 1981; Inglis et al., 2002), 3) the molecular composition of synapses including which receptor-channels reside in the synapse and their dynamic entry into and egress from synapses, and 4) the molecular composition of the postsynaptic density (PSD). The hundreds of proteins in the PSD are the molecular actors that translate synaptic activity into lasting changes in synaptic function. Synaptic activity can play a critical role in synaptic dynamics and one form of activity-dependent development involves activation of the N-methyl-D-aspartate (NMDA) subtype of glutamate receptor (Cline et al.,

686 1987; Kleinschmidt et al., 1987; Kalb, 1994). NMDA-R mediated dendrite growth and synaptic
687 specification involves: 1) elaboration of extracellular factors such as BDNF, Wnts and nitric
688 oxide (Wu et al., 1994; McAllister et al., 1995; Cramer et al., 1996; Inglis et al., 1998; Ha and
689 Redmond, 2008) , 2) activation of intracellular signaling molecules(Wu and Cline, 1998; Li et al.,
690 2000; Li et al., 2002; Redmond et al., 2002; Sin et al., 2002; Yu and Malenka, 2003; Gaudilliere
691 et al., 2004; Wayman et al., 2006; Ha and Redmond, 2008; Peng et al., 2009) and 3) new gene
692 expression(Redmond et al., 2002; Gaudilliere et al., 2004; Shalizi et al., 2006; Li et al., 2009).
693 CRIPT directly and indirectly interacts with multiple components of the PSD and is thus well
694 positioned to modulate neuronal computations.

695

696 *CRIPT interactome*

697 Sequence analysis of CRIPT reveals domain architectures such as zinc-fingers,
698 tetratricopeptide-like helical domains, JmjC domains, and aconitase/3-isopropylmalate
699 dehydratase, swivel domains (see InterPro, EMBL-EBI). Protein interaction databases provide
700 evidence for CRIPT binding to all at least 11 proteins (see IntAct database, EMBL-EBI). These
701 *in silico* and unbiased large-scale screening studies suggest that CRIPT interacts with a wide
702 variety of proteins and may be able to bind DNA and/or double-stranded RNA. Our work shows
703 that CRIPT can be localized to synapses, as well as the cell body, of neurons suggesting CRIPT
704 has important functions in several sites with in the cell.

705 CRIPT binds PDZ3 of synaptic MAGUKs and this interaction is required for association
706 of PSD95 with microtubules (discussed further below)(Passafaro et al., 1999). Other biological
707 actions of CRIPT, such as synaptic clustering of MAGUKs (e.g., PSD95, PSD93 and GKAP)
708 (Passafaro et al., 1999) and dendrite growth (Figure 5) may also depend upon this interaction
709 but this is not known. It is worth noting that both *C.elegans* and *D.melanogaster* CRIPT

710 orthologues have a C-terminal threonine rather than valine (as in mammals). While these two
711 amino acids are sterically similar, there are no known examples of a native PDZ ligand ending in
712 threonine. If exchanging threonine with valine weakens the interaction of worm CRIPT with a
713 PDZ domain-containing protein, it suggests that the biological actions of CRIPT on dendrites
714 could be at least partially independent of a CRIPT/PDZ domain interaction. Future studies will
715 be required to understand which protein-protein interactions subserve CRIPT effects on
716 neurons.

717 Prior work suggests that CRIPT binds microtubules (causing them to bundle) and
718 facilitates recruitment of MAGUKs to bundled microtubules in a heterologous expression system
719 (Niethammer et al., 1998; Passafaro et al., 1999). Since the publication of these studies almost
720 20 years ago a more nuanced view of microtubule binding proteins has emerged and this raises
721 questions about the original observations regarding CRIPT and microtubules. First, whether
722 recombinant CRIPT directly binds purified microtubules has not been demonstrated and so
723 some of the original observations may be due to indirect effects. Second, some proteins that
724 associate with the cytoskeleton, when overexpressed, can decorate microtubules
725 indiscriminately and re-organize with the cellular microtubule network in non-physiological ways.
726 How endogenous CRIPT interacts with microtubules and controls their behavior is unclear.
727 Third, immunogold electron microscopic studies show that CRIPT concentrates in the
728 postsynaptic density along with MAGUKs (Niethammer et al., 1998) and this is consistent with
729 our own immunocytochemical localization studies (Figure 3). On the other hand, large stable
730 microtubules decorated with microtubule associated protein 2 reside in dendritic shafts and are
731 absent from spines (Landis and Reese, 1983; Matus, 2000; Kaech et al., 2001). Even if
732 endogenous CRIPT bound microtubules, the extent to which this occurs at synapses is
733 unknown. We believe that while a stable MAGUK-CRIPT-microtubule complex is unlikely to
734 exist at synapses, these observations do not exclude an ephemeral complex. Dynamic

735 microtubules decorated with plus-end tracking proteins actively explore spines (Gu et al., 2008;
736 Hu et al., 2008; Jaworski et al., 2009; Merriam et al., 2011; 2013). It has been estimated that
737 roughly 1% of spines contain polymerized tubulin at any one time and that every spine will have
738 been invaded by microtubules every 24-hour period (Hu et al., 2008). If CRIPT is truly a
739 microtubule binding protein, it could transiently link invading microtubules to the postsynaptic
740 density.

741

742 *CRIPT cell biology*

743 This work raises a number of issues for future investigation. First, on the basis of the
744 direct physical interaction of CRIPT with SAP97 and other postsynaptic density MAGUKs, does
745 CRIPT influence MAGUK-mediated process such as: 1) clustering and stabilizing glutamate
746 receptors (Chen and Featherstone, 2005; Elias et al., 2007; Waites et al., 2009) , 2) regulating
747 spine size and density (Nikonenko et al., 2008), and 3) trafficking of glutamate receptors to the
748 cell surface (Nicoll et al., 2006; Elias and Nicoll, 2007). Second, several aspects of synaptic
749 biology are influenced by activity and whether CRIPT plays a role in these dynamic processes is
750 an open question. Third, dendritic distribution of CRIPT only partially overlaps with MAGUKs
751 and it is present at some but not all synapses. More advanced imaging technologies may help
752 inform us about the spatio-temporal relationships between CRIPT, synapses and its myriad
753 binding partners. Fourth, do familial mutations in CRIPT impact dendritic and synaptic biology?

754 Understanding how activity-dependent development of the dendritic tree is promoted
755 may help develop tools that can promote recovery following injury to the central nervous
756 system. For instance, repetitive activation of motor circuits in experimental animals or humans
757 has been shown to improve rehabilitation in patients following motor injury (Dietz et al., 1995;
758 Wernig et al., 1995; Edgerton et al., 2001; Gazula et al., 2004; Ivey et al., 2008; Marchal-Crespo

759 and Reinkensmeyer, 2009; Lo et al., 2010). This is consistent with our findings that activity
760 promotes dendritic remodeling that in turn can promote development of normal locomotor
761 behavior (Inglis, et al., 2002; Zhang, et al., 2008; Zhou, et al., 2008).

762

763 **REFERENCES**

764 Brenner, S. (1974). The genetics of Caenorhabditis elegans. Genetics *1*, 71-94.

765

766 Chalfie M, Sulston J (1981) Developmental genetics of the mechanosensory neurons of
767 Caenorhabditis elegans. Dev Biol 82:358–370.

768

769 Chen K, Featherstone DE (2005) Discs-large (DLG) is clustered by presynaptic innervation and
770 regulates postsynaptic glutamate receptor subunit composition in Drosophila. BMC Biol 8;3:1.

771

772 Cline HT, Debski EA, Constantine-Paton M (1987) N-methyl-D-aspartate receptor antagonist
773 desegregates eye-specific columns. PNAS 84:4342–4345.

774

775 Cramer KS, Angelucci A, Hahm J-O, Bogdanov MB, Sur M (1996) A role for nitric oxide in the
776 development of the ferret retinogeniculate projection. J Neurosci 16:7995–8004.

777

778 Dietz V, Colombo G, Jensen L, Baumgartner L (1995) Locomotor capacity of spinal cord in
779 paraplegic patients. Ann Neurol 37: 574-582.

780

781 Edgerton VR, Leon RD, Harkema SJ, Hodgson JA, London N, Reinkensmeyer DJ, et al. (2001)
782 Retraining the injured spinal cord. J Physiol 533: 15-22.

783

784 Elias GM, Funke L, Stein V, Grant SG, Bredt DS, Nicoll RA (2007) Synapse-specific and
785 developmentally regulated targeting of AMPA receptors by a family of MAGUK scaffolding
786 proteins. Neuron 52: 307-320.

787

788 Elias, G. M., & Nicoll, R. A. (2007). Synaptic trafficking of glutamate receptors by MAGUK
789 scaffolding proteins. *Trends Cell Biol*, *17*(7), 343–352.

790

791 Gaudilliere B, Konishi Y, la Iglesia de N, Yao G, Bonni A (2004) A CaMKII-NeuroD signaling
792 pathway specifies dendritic morphogenesis. Neuron 41:229–241.

793

794 Gazula VR, Roberts M, Luzzio C, Jawad AF, Kalb RG (2004) Effects of limb exercise after
795 spinal cord injury on motor neuron dendrite structure. J Comp Neurol 476: 130-145.

796

797 Gu J, Firestein BL, Zheng JQ (2008) Mictotubules in dendritic spine development. J Neurosci
798 28: 12120-4.

799

800 Ha S, Redmond L (2008) ERK mediates activity dependent neuronal complexity via sustained
801 activity and CREB-mediated signaling. Dev Neurobiol 68:1565–1579.

802

803 Haas K, Li J, Cline HT (2006) AMPA receptors regulate experience-dependent dendritic arbor
804 growth in the intact brain. Proc. Natal. Acad. Sci. 103: 12127-12131.

805

806 Howard MA, Elias GM, Elias LA, Swat W, Nicoll RA (2010) The role of SAP97 in synaptic
807 glutamate receptor dynamics. Proc. Natl. Acad. Sci. 107: 3805-3810.

808

809 Hu X, Viesselmann C, Nam S, Merriam E, Dent EW (2008) Activity-dependent dynamic
810 microtubule invasion of dendritic spines. J Neurosci 28: 13094-105.

811

812 Hume RI, Purves D (1981) Geometry of neonatal neurons and the regulation of synapse
813 elimination. Nature 293:469–471.

814

815 Hung AY, Sheng M (2002) PDZ domains: structural modules for protein complex assembly. J
816 Biol Chem 277:5699–5702.

817

818 Inglis FM, Furia F, Zuckerman KE, Strittmatter SM, Kalb RG (1998) The role of nitric oxide and
819 NMDA receptors in the development of motor neuron dendrites. J Neurosci 18:10493–10501.

820

821 Inglis, FM, Crockett R, Korada S, Abraham WC, Hollmann M, Kalb RG (2002) The AMPA
822 receptor subunit GluR1 regulates dendritic architecture of motor neurons. J. Neurosci. 22: 8042-
823 8051.

824

825 Irie M, Hata Y, Takeuchi M, Ichtchenko K, Toyoda A, Hirao K, Takai Y, Rosahl TW, Sudhof TC
826 (1997) Binding of Neuroligins to PSD-95. Science 277:1511–1515.

827

828 Ivey FM, Hafer-Macko CE, Macko RF (2008) Task-oriented treadmill exercise training in chronic
829 hemiparetic stroke. J Rehabil Res Dev. 45(2):249-59

830

831 Jablonski AM, Kalb RG (2013) GluA1 promotes the activity-dependent development of motor
832 circuitry in the developing spinal cord. An N Y Acad Sci 1279: 54-59.

833

834 Jakowec MW, Fox AJ, Martin LJ, Kalb RG (1995a) Quantitative and qualitative changes in
835 AMPA receptor expression during spinal cord development. Neuroscience 67: 893-907.

836

837 Jakowec MW, Yen L, Kalb RG (1995b) In situ hybridization analysis of AMPA receptor subunit
838 gene expression in the developing rat spinal cord. Neuroscience 68: 909-920.

839

840 Jaworski J, Kapitein LC, Gouveia SM, Dortland BR, Wulf PS, Grigoriev I, Camera P, Spangler
841 SA, Di Stefano P, Demmers J, Krugers H, Defilippi P, Akhmanova A, Hoogenraad CC (2009)
842 Dynamic microtubules regulate dendritic spine morphology and synaptic plasticity. Neuron
843 61:85–100.

844

845 Jeong GB, Werner M, Gazula VR, Itoh T, Roberts M, David S, Pfister B, Cohen A, Neve RL,
846 Hollmann M, Kalb RG (2006) Bi-directional control of motor neuron dendrite remodeling by the
847 calcium permeability of AMPA receptors. Mol. Cell. Neurosci. 32: 299-314.

848

849 Kaech S, Parmar H, Roelandse M, Bornmann C, Matus A (2001) Cytoskeletal
850 microdifferentiation: a mechanism for organizing morphological plasticity in dendrites. PNAS 98:
851 7086-7092.

852

853 Kalb RG (1994) Regulation of motor neuron dendrite growth by NMDA receptor activation.
854 Development 120: 3063-3071.

855

856 Kaletsky R, Lakhina V, Arey R, Williams A, Landis J, Ashraf J, Murphy CT (2016) The C.
857 elegans adult neuronal IIS/FOXO transcriptome reveals adult phenotype regulators. Nature
858 529:92–96.

859

860 Kim CH, Takamiya K, Petralia RS, Sattler R, Yu S, Zhou W, Kalb R, Wenthold R, Huganir R.
861 (2005) Persistent hippocampal CA1 LTP in mice lacking the C-terminal PDZ ligand of GluR1.
862 Nat. Neurosci. 8: 985-987.

863

864 Kleinschmidt A, Bear MF, Singer W (1987) Blockade of “NMDA” receptors disrupts experience-
865 dependent plasticity of kitten striate cortex. Science 238:355–358

866

867 Landis DM, Reese TS (1983) Cytoplasmic organization in cerebellar dendritic spines. J Cell Biol
868 97: 1169-1178.

869

870 Leduc MS, Niu Z, Bi W, Zhu W, Miloslavskaya I, Chiang T, Streff H, Seavitt JR, Murray SA, Eng
871 C, Chan A, Yang Y, Lalani SR (2016) CRIPT exonic deletion and a novel missense mutation in
872 a female with short stature, dysmorphic features, microcephaly, and pigmentary abnormalities.
873 Am J Med Genet A 170:2206–2211.

874

875 Li S, Zhang C, Takemori H, Zhou Y, Xiong ZQ (2009) TORC1 regulates activity-dependent
876 CREB-target gene transcription and dendritic growth of developing cortical neurons. J Neurosci
877 29:2334–2343.

878

879 Li Z, Aizenman CD, Cline HT (2002) Regulation of rho GTPases by crosstalk and neuronal
880 activity in vivo. Neuron 33:741–750.

881

882 Li Z, Van Aelst L, Cline HT (2000) Rho GTPases regulate distinct aspects of dendritic arbor
883 growth in Xenopus central neurons in vivo. Nat Neurosci 3:217–225.

884

885 Liu OW, Shen K. (2011) The transmembrane LRR protein DMA-1 promtoes dendrite branching
886 and growth in C. elegans. Nature Neuroscience 15: 57-63.

887 Ivey FM, Hafer-Macko CE, Macko RF (2008) Task-oriented treadmill exercise training in
888 chronic hemiparetic stroke. J Rehabil Res Dev. 45(2):249-59.

889

890 Lo AC, Guarino PD, Richards LG, Haselkorn JK, Wittenberg GF, Rederman DG, et al. (2010)
891 Robot-assisted therapy for long-term upper limb impairment after stroke. N Engl J Med 362:
892 1772-1783.

893

894 McAllister AK, Lo DC, Katz LC (1995) Neurotrophins regulate dendritic growth in developing
895 visual cortex. Neuron 15:791–803.

896

897 Marchal-Crespo L, Reinkensmeyer DJ (2009) Review of control strategies for robotic movement
898 training after neurologic injury. J Neuroeng Rehabil 6:20.

899

900 Matus A (2000) Actin-based plasticity in dendritic spines. Science 290: 754-758.

901

902 Merriam EB, Lumbard DC, Viesselmann C, Ballweg J, Stevenson M, Pietila L, et al. (2011)
903 Dynamic microtubules promote synaptic NMDA receptor-dependent spine enlargement. PLoS
904 One 6: e27688.

905

906 Merriam EB, Millette M, Lumbard DC, Saengsawang W, Fothergill T, Hu X, et al. (2013)
907 Synaptic regulation of microtubule dynamics in dendritic spines by calcium, F-actin, and drebrin.
908 J Neurosci 33: 16471-82.

909

910 Micheva, K. D., Busse, B., Weiler, N. C., O'Rourke, N., & Smith, S. J. (2010). Single-synapse
911 analysis of a diverse synapse population: proteomic imaging methods and markers. *Neuron*,
912 *68*(4), 639–653.

913

914 Midgley CA, White S, Howitt R, Save V, Dunlop MG, Hall PA, Lane DP, Wyllie AH, Bubb VJ
915 (1997) APC expression in normal human tissues. J Pathol 181: 426-433.

916

917 Moore JH, Dupuy D, Vidal M (2005) A gene expression fingerprint of C. elegans embryonic
918 motor neurons. BMC Genomics 6:42

919

920 Neve, R L. Howe, J R. Hong, S. Kalb, R G. (1997): Introduction of the glutamate receptor
921 subunit 1 into motor neurons in vitro and in vivo using a recombinant herpes simplex virus.
922 Neuroscience 79(2): 435-47

923

924 Ni X, Martin-Caraballo M (2010) Differential effect of glutamate receptor blockade on dendritic
925 outgrowth in chicken lumbar motoneurons. Neuropharmacology 58: 593-604.

926

927 Nicoll RA, Tomita S, Bredt DS (2006) Auxiliary subunits assist AMPA-type glutamate receptors.
928 Science 311:1253–1256.

929

930 Niethammer M, Valtschanoff JG, Kapoor TM, Allison DW, Weinberg RJ, Craig AM, Sheng M
931 (1998) CRIPT, a novel postsynaptic protein that binds to the third PDZ domain of
932 PSD95/SAP90. Neuron (4): 693-707.

933

934 Nikonenko I, Boda B, Steen S, Knott G, Welker E, Muller D (2008) PSD-95 promotes
935 synaptogenesis and multiinnervated spine formation through nitric oxide signaling. J Cell Biol
936 183:1115–1127.

937

938 Passafaro M, Sala C, Niethammer M, Sheng M (1999) Microtubule binding by CRIPT and its
939 potential role in the synaptic clustering of PSD95. Nat Neurosci (12): 1069-1069.

940

941 Peng YR, He S, Marie H, Zeng SY, Ma J, Tan ZJ, Lee SY, Malenka RC, Yu X (2009)
942 Coordinated changes in dendritic arborization and synaptic strength during neural circuit
943 development. Neuron 61:71–84.

944

945 Redmond L, Kashani AH, Ghosh A (2002) Calcium regulation of dendritic growth via CaM
946 kinase IV and CREB-mediated transcription. Neuron 34:999–1010.

947

948 Sans N, Racca C, Petralia RS, Wang YX, McCallum J, Wenthold RJ (2001) Synapse-
949 associated protein 97 selectively associates with a subset of AMPA receptors early in their
950 biosynthetic pathway. J Neurosci 21:7506–7516.

951

952 Schlüter OM, Xu W, Malenka RC (2006) Alternative N-terminal domains of PSD95 and SAP97
953 govern activity-dependent regulation of synaptic AMPA receptor function. Neuron 51: 99-111.

954

955 Shaheen R, Fageih E, Ansari S, Abdel-Salam G, Al-Hassnan ZN, Al-Shidi T, Almoar R, Sogaty
956 S, Alkuraya FS (2014) Genomic analysis of primordial dwarfism reveals novel disease genes.
957 Genome Res 24: 291-299.

958

959 Shalizi A, Gaudilliere B, Yuan Z, Stegmuller J, Shirogane T, Ge Q, Tan Y, Schulman B, Harper
960 JW, Bonni A (2006) A calcium-regulated MEF2 sumoylation switch controls postsynaptic
961 differentiation. Science 311:1012–1017.

962

963 Sin WC, Haas K, Ruthazer ES, Cline HT (2002) Dendrite growth increased by visual activity
964 requires NMDA receptor and Rho GTPases. Nature 419:475–480.

965

966 Smith CJ, Watson JD, Spencer WC, O'Brien T, Cha B, Albeg A, Treinin M, Miller DM 3rd.
967 (2010) Time-lapse imaging and cell-specific expression profiling reveal dynamic branching and
968 molecular determinants of a multi-dendritic nociceptor in C. elegans. Dev Bio 345: 18-33.

969

970 Smith CJ, O'Brien T, Chatzigeorgiou M, Spencer WC, Feingold-Link E, Husson SJ, Hori S,
971 Mitani S, Gottschalk A, Schafer WR, Miller DM 3rd. (2013) Sensory neuron fates are
972 distinguished by a transcriptional switch that regulates dendrite branch stabilization. Neuron 79:
973 266-280.

974

975 Söderberg O, Gullberg M, Jarvius M, Ridderstråle K, Leuchowius K-J, Jarvius J, Wester K,
976 Hydbring P, Bahram F, Larsson L-G, Landegren U (2006) Direct observation of individual
977 endogenous protein complexes in situ by proximity ligation. Nat Methods 3:995–1000.

978

979 Stegenga SL and Kalb RG (2001) Developmental regulation of N-methyl-D-aspartate- and
980 kainite-type glutamate receptor expression in the rat spinal cord. Neuroscience 105: 499-507.

981

982 Stetina Von SE, Watson JD, Fox RM, Olszewski KL, Spencer WC, Roy PJ, Miller DM (2007)
983 Cell-specific microarray profiling experiments reveal a comprehensive picture of gene
984 expression in the C. elegans nervous system. Genome Biol 8:R135.

985

986 Stuart G., Spruston, N., and Häusser, M. (1999) Dendrites. Oxford University Press

987

988 Waites CL, Specht CG, Hartel K, Leal-Ortiz S, Genoux D, Li D, Drisdel RC, Jeyifous O, Cheyne
989 JE, Green WN, Montgomery JM, Garner CC (2009) Synaptic SAP97 isoforms regulate AMPA
990 receptor dynamics and access to presynaptic glutamate. J Neurosci 29:4332–4345.

991

992 Way JC, Chalfie M. (1989) The mec-3 gene of Caenorhabditis elegans requires its own product
993 for maintained expression and is expressed in three neuronal cell types. Genes Dev. 3: 1823-
994 1833.

995

996 Wayman GA, Impey S, Marks D, Saneyoshi T, Grant WF, Derkach V, Soderling TR (2006)
997 Activity-dependent dendritic arborization mediated by CaM-kinase I activation and enhanced
998 CREB-dependent transcription of Wnt-2. Neuron 50:897–909.

999

1000 Wernig A, Muller S, Nanassy A, Cagol E (1995) Laufband therapy based on “rules of spinal
1001 locomotion” is effective in spinal cord injured persons. Eur J Neurosci 7: 823-9.

1002

1003 Wu GY, Cline HT (1998) Stabilization of dendritic arbor structure in vivo by CaMKII. Science
1004 279:222–225.

1005

1006 Wu HH, Williams CV, McLoon SC (1994) Involvement of nitric oxide in the elimination of a
1007 transient retinotectal projection in development. Science 265:1593–1596.

1008

1009 Yu X, Malenka RC (2003) |[beta]|-catenin is critical for dendritic morphogenesis. Nature
1010 Neuroscience 6:1169–1177.

1011

1012 Zhang L, Hsu FC, Mojsilovic-Petrovic J, Jablonski AM, Zhai J, Coulter DA, Kalb RG (2015)
1013 Structure-function analysis of SAP97, a modular scaffolding protein that drives dendrite growth.
1014 Mol. Cell Neurosci. 65: 31-44.

1015

1016 Zhang L, Schessl J, Werner M, Bonnemann C, Xiong G, Mojsilovic-Petrovic J, Zhou W, Cohen
1017 A, Seeburg P, Misawa H, Jayaram A, Personius K, Hollmann M, Sprengel R, Kalb RG (2008)
1018 Role of GluR1 in activity-dependent motor system development. J. Neurosci. 28: 9953-9968.

1019

1020 Zhou W, Zhang L, Guoxiang X, Mojsilovic-Petrovic J, Takamaya K, Sattler R, Huganir R, Kalb
1021 RG (2008) GluR1 controls dendrite growth via its binging partner, SAP97. J Neurosci. 28:
1022 10220-10233.

1023

FIGURE LEGENDS

Figure 1. CRIPT is *bona fide* PDZ3 and SAP97 interacting protein. (A) Amino acid sequence alignment of the PDZ3 domains of human SAP97 and human PSD95; there is 86% identity. Residues highlighted in yellow indicate amino acids directly involved in binding the C-terminus of CRIPT. Arrows and cylinders above the amino acid sequence indicate secondary structure of the PDZ domain (i.e., βA means beta strand A, αA means alpha helix A, etc.), (B) Full-length (FL) myc-tagged SAP97 co-immunoprecipitates with FL HA-tagged CRIPT using the anti-HA antibody when they are overexpressed in HEK293 cells. Neither protein immunoprecipitates with a negative control IgG. (C) Overexpressed HA-tagged CRIPT co-immunoprecipitates with myc-tagged SAP97 containing a mutation in the PDZ2 domain (K323A, K326A), but mutation of the PDZ3 domain (H469A, R470A) disrupts this interaction. (D) Overexpression of myc-tagged full-length SAP97 and full-length WT CRIPT or full-length CRIPT V101A in HEK293 cells and immunoprecipitation SAP97 using myc IgG. Mutating the PDZ3-interaction motif of CRIPT (CRIPT V101A) abolishes the interaction between SAP97 and CRIPT. (E) anti-SAP97 (but not a control IgG) Immunoprecipitates WT or PDZ3 mutant version of SAP97 equivalently from cell lysates, as revealed by assay for supernatant post IP. Full-length SAP97 interacts with full-length APC protein in HEK293 cells, but this interaction does not rely on a ligand-binding PDZ3 domain in SAP97. (F) Full-length CRIPT interacts with the PDZ3 domain of SAP97 in a yeast-two-hybrid assay. (G) Surface plasmon resonance (SPR) shows a specific and saturable interaction between the 18 C-terminal amino acids of CRIPT and the PDZ3 domain of SAP97 (K_d of 6.57μM), but no interaction when the CRIPT V101A mutation is present. Values shown were subtracted by a negative control GST peptide. (H) Endogenous CRIPT and endogenous SAP97 co-immunoprecipitate in lysates prepared from DIV14 mixed spinal cultures. Immunoblotting of endogenous SAP97 and CRIPT proteins in input lysate and

1049 immunoprecipitations using a negative control IgG and CRIPT IgG. Blot was incubated with
1050 SAP97 and CRIPT antibody simultaneously.

1051 **Figure 2: Structural model of SAP97 PDZ3 in complex with the CRIPT C-terminal tail.** (A)
1052 The SAP97 PDZ3/CRIPT peptide complex structure modeled using the experimentally derived
1053 PSD95 PDZ3/CRIPT complex structure (PDB id:1BE9) depicted in (B). In these drawings, the
1054 CRIPT peptide is depicted in purple.

1055 **Figure 3. CRIPT partially co-localizes synaptophysin containing synapses.** Mixed spinal
1056 cord cultures at DIV21 were immunocytochemically analyzed. The first row of panels show
1057 immunocytochemical staining for HA-CRIPT (red), synaptophysin (green) and both together in
1058 the merge image. HA-CRIPT immunoreactivity is seen within the soma and throughout the
1059 dendritic tree. This localization data matches what was previously reported (Niethammer et al.,
1060 1998b). Calibration bar = 20 microns. Beneath each of the lower power images are higher
1061 magnification images of the area outlined in a white box. In the high power HA-CRIPT panel,
1062 immunocytochemically positive material is seen in various morphologies within the dendritic tree
1063 including small or large round puncta and elongated dendritic shaft entities. HA-CRIPT appears
1064 inhomogenously within dendritic outgrowths that may represent spines or filopodia. In the
1065 merge image, areas of overlap (HA-CRIPT + synaptophysin) are yellow and are highlighted with
1066 “>”. (Calibration bar = 5.0 microns). These are likely to represent synapses.

1067

1068 **Figure 4. CRIPT partially co-localizes GluA1 positive and SAP97 positive puncta on**
1069 **dendrites.** Mixed spinal cord cultures at DIV21 were immunocytochemically analyzed. The
1070 upper set of panels display images of HA-CRIPT and EGFP-SAP97 and the lower set of panels
1071 display images of HA-CRIPT and GluA1. For the HA-CRIPT/EGFP-SAP97 panels, the first row
1072 of panels show immunocytochemical staining for HA-CRIPT (red), EGFP-SAP97 (green) and

merge. As in Figure 3, HA-CRIPT immunoreactivity is seen within the soma and throughout the dendritic tree. EGFP-SAP97 is similarly distributed but appears more punctate. In the merge image, extensive co-localization is seen (yellow) both in the soma and the dendritic tree. Calibration bar = 30 microns. Beneath each of the lower power images are higher magnification images of the area outlined in a white box. In the high power HA-CRIPT panel, immunocytochemically positive material is again seen in various morphologies within the dendritic tree including small or large round puncta and elongated dendritic shaft entities. HA-CRIPT appears inhomogenously within dendritic outgrowths that may represent spines or filopodia. EGFP-SAP97 is clearly more punctate than HA-CRIPT and in the merge image areas of colocalization are seen (yellow, denoted with ">"). EGFP-SAP97 appears enriched at along the edges of HA-CRIPT immunoreactivity. Calibration bar = 10 microns. For the HA-CRIPT/GluA1 panels, the first row of panels show immunocytochemical staining for HA-CRIPT (red), GluA1 (green) and merge. Again, HA-CRIPT immunoreactivity is seen within the soma and throughout the dendritic tree. GluA1 is seen exclusively as puncta. In the merge image, co-localization is seen (yellow) in the dendritic tree. Calibration bar = 20 microns. Beneath each of the lower power images are higher magnification images of the area outlined in a white box. In the high power HA-CRIPT panel, immunocytochemically positive material is again seen in various morphologies within the dendritic tree including small or large round puncta and elongated dendritic shaft entities. HA-CRIPT appears inhomogenously within dendritic outgrowths that may represent spines or filopodia. GluA1 is exclusively punctate and in the merge image areads of colocalization are seen (yellow, denoted with ">"). GluA1, like EGFP-SAP97, appears enriched at along the edges of HA-CRIPT immunoreactivity. (Calibration bar = 4.0 microns).

Figure 5. CRIPT is necessary, but not sufficient, for the dendritic growth of spinal cord neurons. Mixed spinal cord cultures were used for biochemistry and morphometry. (A) DIV14 cultures were infected with HSV engineered to express a miRNA that targets CRIPT or a scrambled sequence control. Lysates were probed for CRIPT and the miRNA to CRIPT reduces the abundance of CRIPT by western blot compared to a scrambled miRNA. (B) Knockdown of CRIPT results in a significant decrease in a decrease in the number of branches and total dendritic length of the dendritic tree. No other dendritic parameter was different between groups. *Differs from +GFP group, $p < 0.05$; †Differs from +scrambled miRNA group, $p < 0.05$. (C) HEK 293 cells were transfected with plasmids engineered to express miRNA targeted to CRIPT (or scrambled sequence control) and WT-CRIPT ($CRIPT^{WT}$) or a miRNA-resistant version of CRIPT ($CRIPT^{res}$). When lysates were probed for CRIPT we saw reduced abundance of $CRIPT^{WT}$ but not the $CRIPT^{res}$ by the miRNA targeted to CRIPT. (D) Co-transfection of RNAi-resistant CRIPT is sufficient to prevent decrease in the number of branches and total length of the dendritic tree by CRIPT miRNA. *Differs from +GFP group, $p < 0.05$; †Differs from +CRIPT miRNA group, $p < 0.05$. CRIPT was modified with a sequence from paralemin-1 to allow for palmitoylation was generated. (E) HEK293 cells were transfected a plasmid engineered to express $CRIPT^{WT}$ or palmitoylated CRIPT, and cells were lysed and fractionated to enrich for the cytosol or membrane fractions. Western blots for CRIPT show that $CRIPT^{WT}$ is predominantly in the cytosolic fraction and palmitoylated CRIPT is predominantly in the membrane fraction. (F) Overexpression of WT CRIPT or pal-myc CRIPT has no effect on the size or complexity of the dendritic tree compared with GFP only expressing neurons.

Figure 6. CRIPT functions downstream of SAP97 in promoting dendrite growth. . Mixed spinal cord cultures were used for morphometry. Knockdown of CRIPT prevents growth and branching caused by SAP97 overexpression in mixed spinal cord neurons. *Differs from +GFP group, $p < 0.05$; †Differs from +SAP97 + +scrambled miRNA group, $p < 0.05$.

Figure 7 CRIPT knockdown leads to a selective reduction in the abundance of GluA1 and SAP97. Mixed spinal cord cultures were infected with HSV engineered to express a miRNA targeting CRIPT or a scrambled control. Two days later, lysates were prepared and subjected to western blots. No less than 6 independent experiments were performed for the quantitative image analysis. CRIPT knockdown leads to a reduction in GluA1 and SAP97 abundance and no effect on the abundance of GluA2, GluA4, NR1, NR2A, NR2B or PSD95. Representative images of Western blots with actin loading controls are shown and quantification of band intensity in the bar graphs below. * significant difference between groups, $p < 0.05$.

Figure 8. Loss of *cript* (*tm430*) decreases dendrite branch number *in vivo* and results in a mechanosensory defect; rescue with human CRIPT (A) Representative full body image of PVD neuron labeled with GFP in a N2 Bristol strain (wild type; "wt") young adult (L4 stage + 1 day old). (B) Schematic of PVD neuron and its primary (1˚), secondary (2˚), and tertiary (3˚) branches used for quantification. (C) Representative images of the PVD neuron labeled with GFP of indicated genotypes in the tail region used for quantification at the young adult stage (L4 stage + 1 day old). Gaps in the dendritic tree of *cript* (*tm430*) worms are noted with "v". (D) Quantification of the number of primary (1˚), secondary (2˚), and tertiary (3˚) branches in indicated strains (n ≥ 10 per genotype). Analyst was blinded to genotype during quantification. We found that *cript* (*tm430*) mutants have a significant decrease in secondary (**$p < 0.01$; *post hoc* test following one-way ANOVA) ($F_{(3,37)} = 6.781$; $p = 0.0009$) and tertiary (**$p < 0.01$; *post hoc* test following one-way ANOVA) ($F_{(3,37)} = 6.365$; $p = 0.0014$) branch number. This was completely rescued by overexpression of the human ortholog of CRIPT in the nervous system using the unc-119 promoter (P_{neuron}) which also increased the number of primary dendrites compared to N2 (WT) (*$p < 0.05$; *post hoc* test following one-way ANOVA) ($F_{(3,37)} = 3.569$; $p = 0.0232$). (E) WT (N2 Bristol strain), *cript* (*tm430*), *mec-3 (e1338)*, and *cript* (*tm430*); *mec-4* (*tu253)* animals were scored for their response to touch. Average of 3 independent experiments

is shown. Experiments were all completed with analyst blinded to genotype. We found that *cript* (*tm430*); *mec-4* (*tu253*) animals show a synthetic touch defect (**p <0.01 according to a *post hoc* test following a one-way ANOVA). We also confirmed that mec-3 (CB1338) animals are touch defective compared to wild type (N2) counterparts (***p < 0.005 according to a *post hoc* test following a one-way ANOVA) ($F_{(4,10)}$ = 11.93; p = 0.0008). (F) Touch defect is suppressed in *cript* (*tm430*); *mec-4* (*tu253*) animals by overexpression of the human ortholog of CRIPT in the nervous system using the unc-119 promoter (P_{neuron}::hCRIPT) in four independent extrachromasomal array lines (**p <0.01 according to a *post hoc* test following a one-way ANOVA when compared to non-transgenic counterparts). One strain (line 1) fully rescued the touch defect when compared to wild type (N2) in a *post hoc* test following a one-way ANOVA ($F_{(8,18)}$ = 26.45; p < 0.0001).

Figure 1

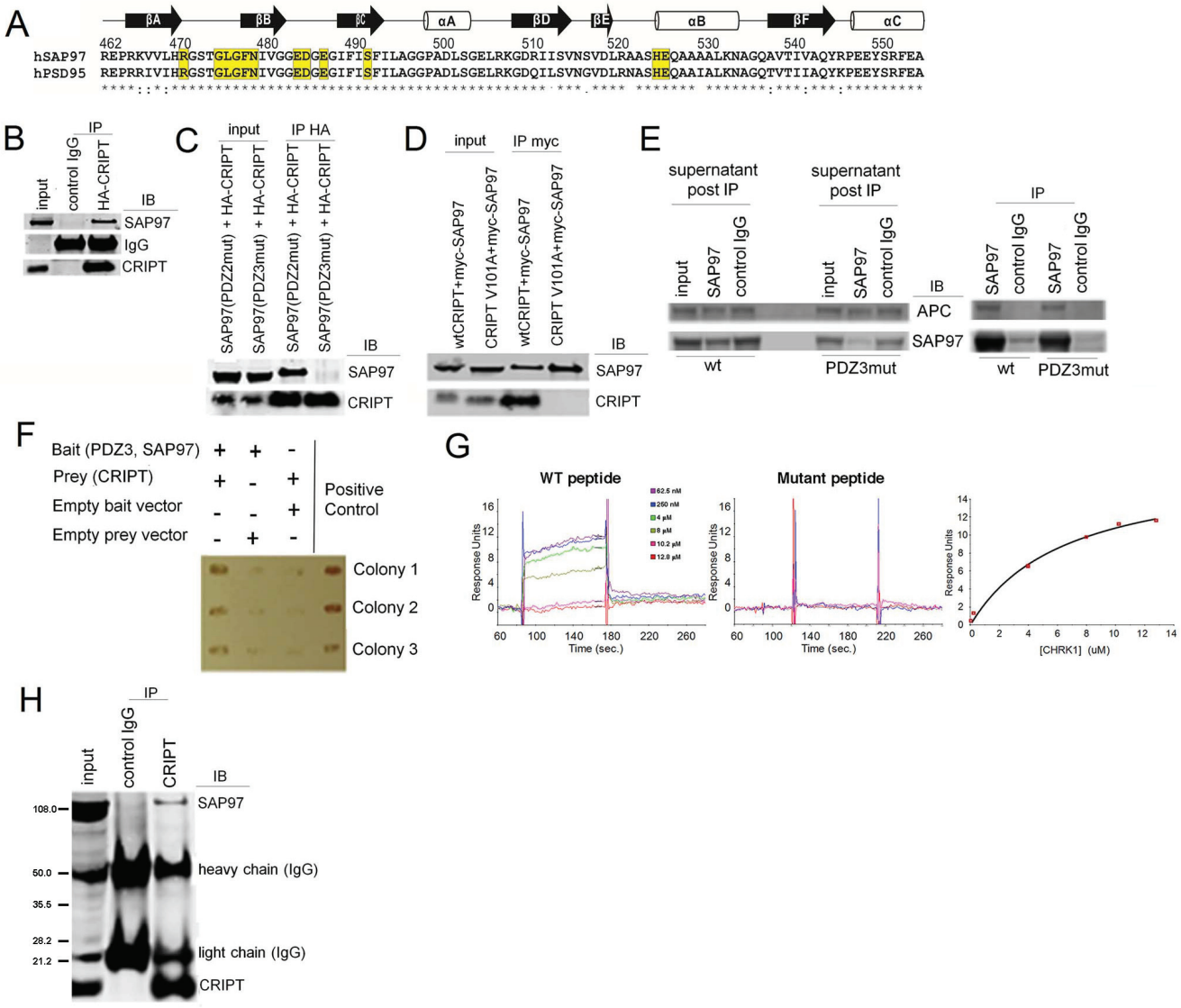

Figure 2

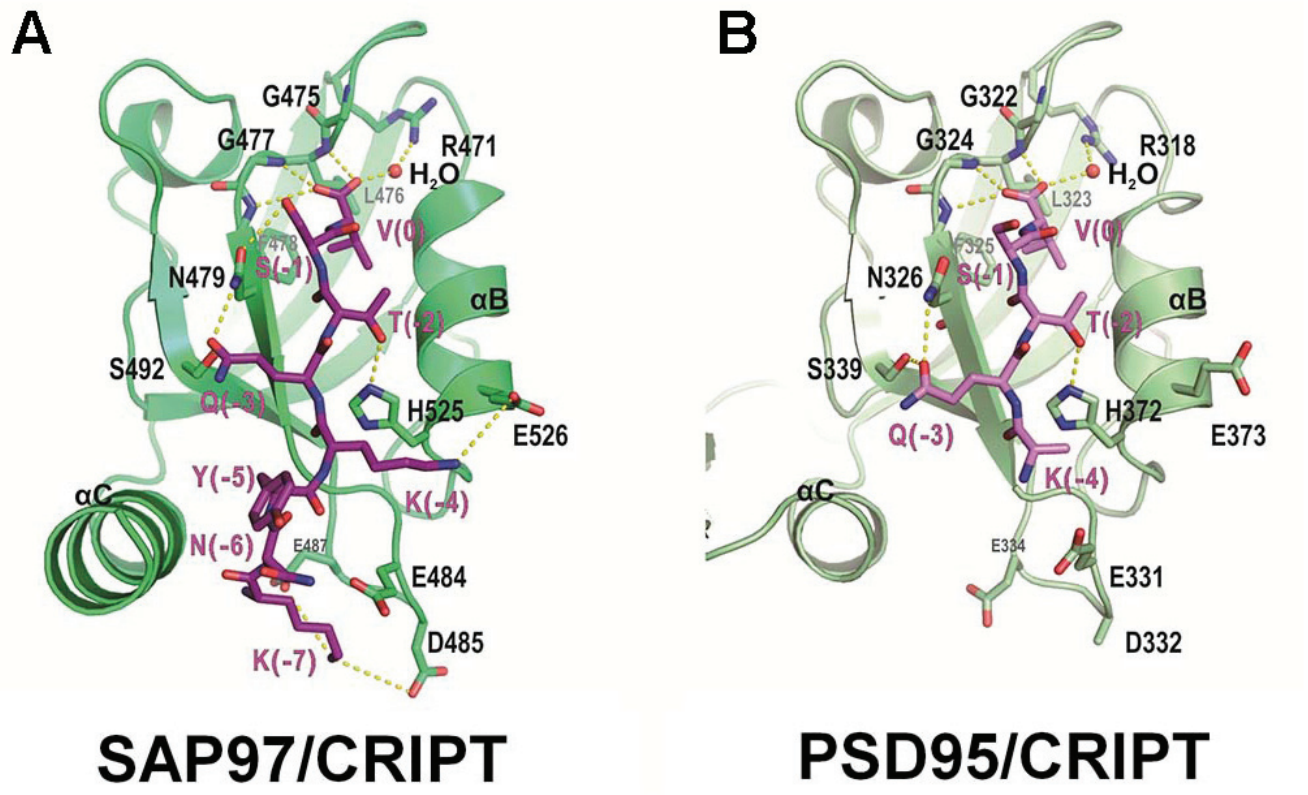

Figure 3

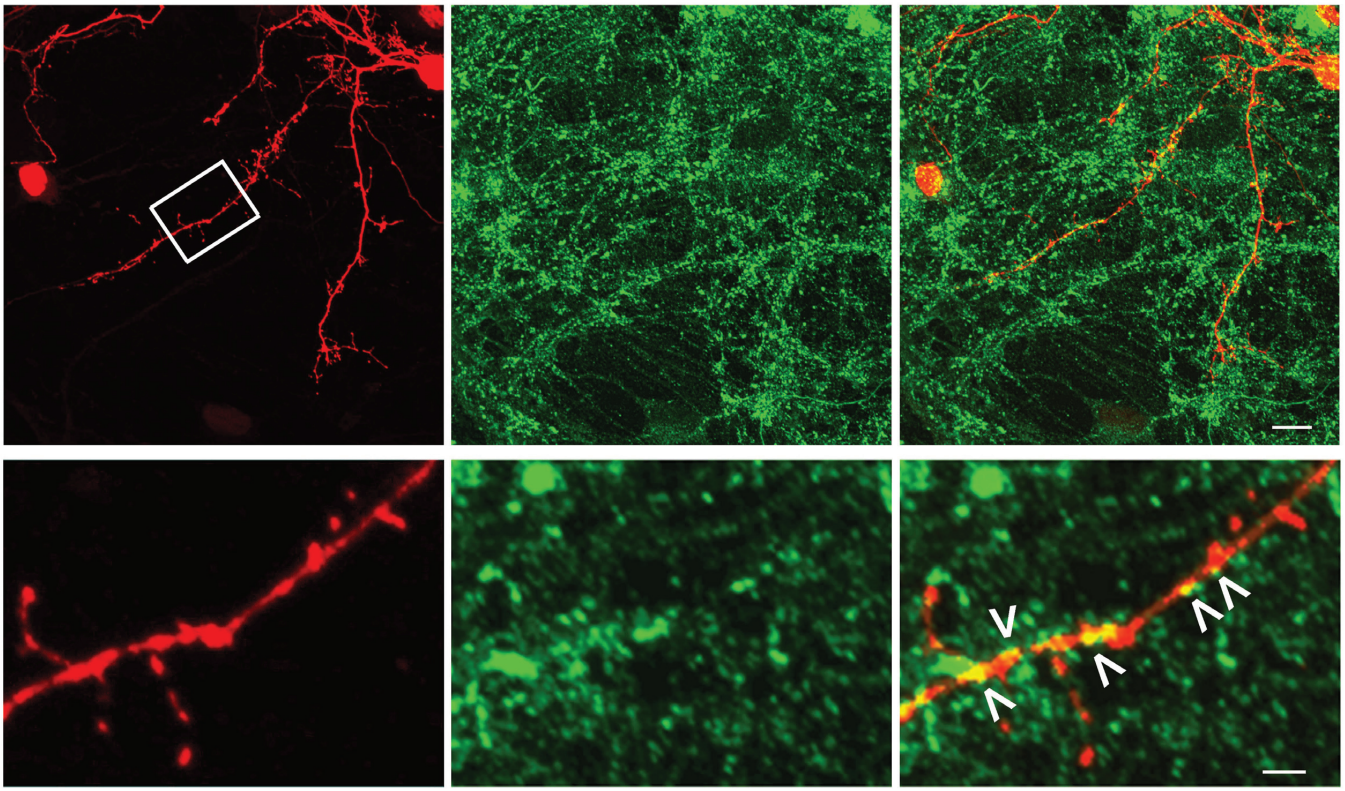

Figure 4

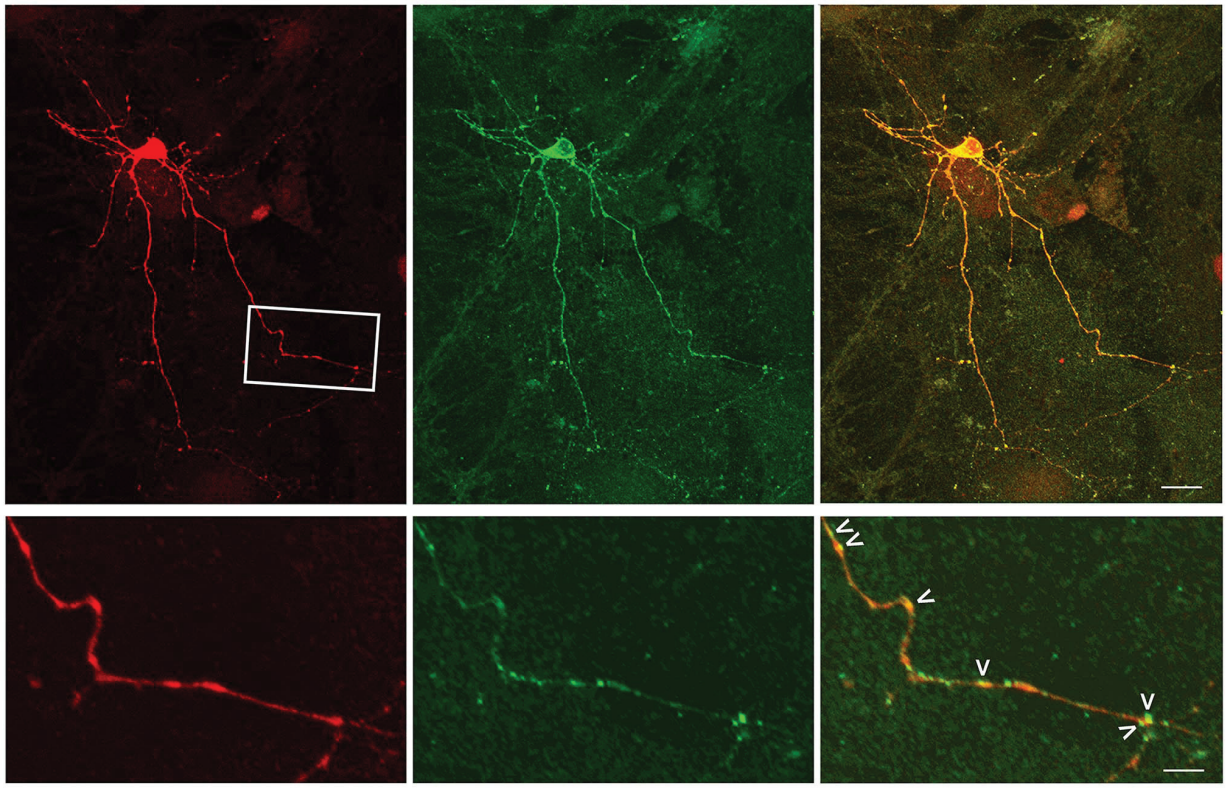

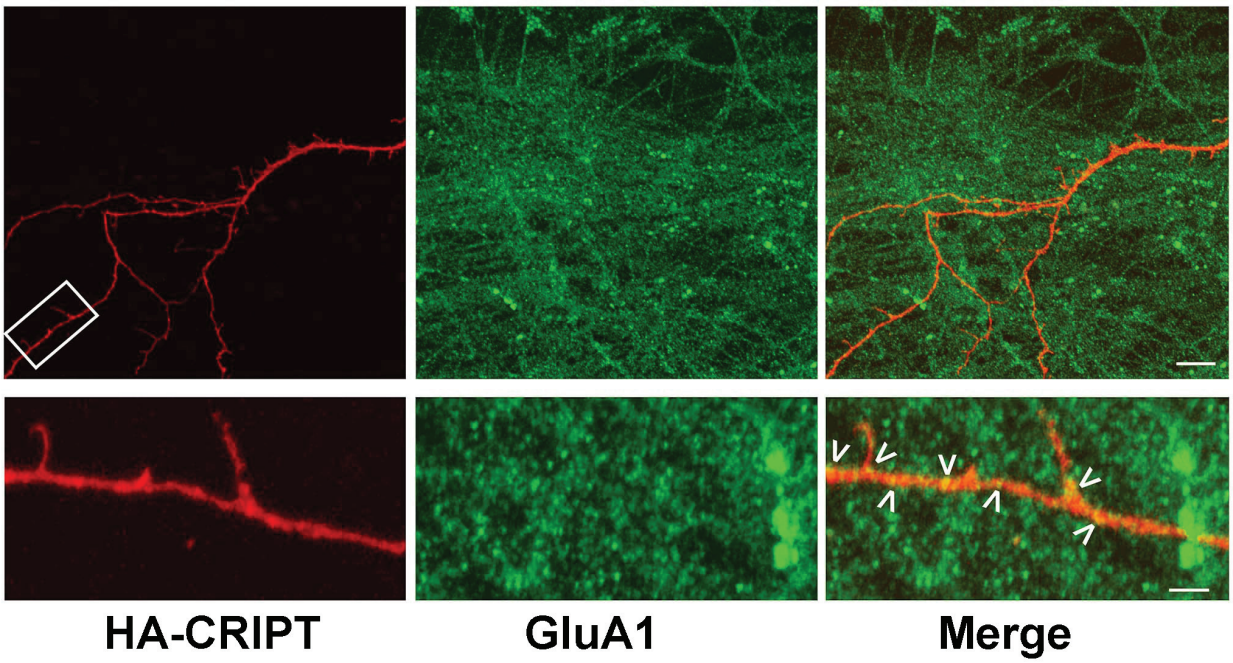

Figure 5

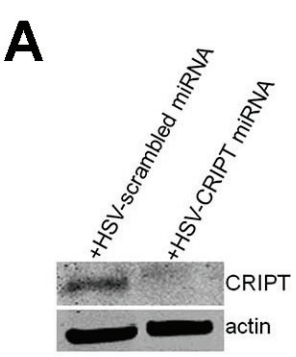

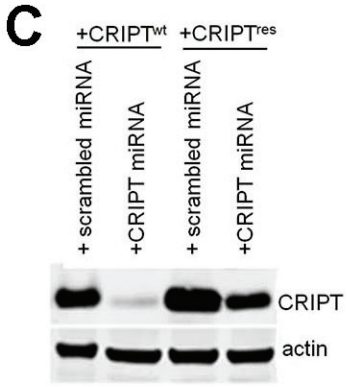

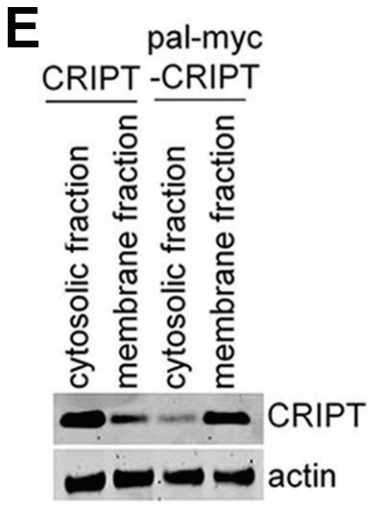

B

+GFP | +scrambled miRNA | +CRIPT miRNA

Cell Parameter	+GFP (n = 26)	+scrambled miRNA (n = 25)	+CRIPT miRNA (n = 25)	*p*
Soma area (μm²)	217 ± 7Δ	212 ± 8	228 ± 14	0.799
1⁰ dendrites, #	6.4 ± 0.3	6.5 ± 0.4	5.7 ± 0.3	0.179
Branches, #	16.3 ± 0.9	18.4 ± 0.9	13.6 ± 1.0†	0.001
∑length (μm)	1036 ± 40	982 ± 35	848 ± 39*†	0.002
Average dendrites (μm)	171 ± 10	159 ± 8	156 ± 10	0.330
Longest dendrite (μm)	170 ± 7	158 ± 9	177 ± 11	0.295

D

+scrambled miRNA | +CRIPT miRNA | +CRIPT miRNA +CRIPTres

Cell Parameter	+scrambled miRNA (n = 26)	+CRIPT miRNA (n = 25)	+CRIPT miRNA +CRIPTres (n = 25)	*p*
Soma area (μm²)	303 ± 16Δ	281 ± 22	275 ± 16	0.295
1⁰ dendrites, #	6.0 ± 0.3	5.6 ± 0.3	6.5 ± 0.4	0.213
Branches, #	12.2 ± 0.9	9.6 ± 0.6*	13.7 ± 1.0†	0.007
∑length (μm)	1046 ± 72	792 ± 36*	956 ± 53†	0.009
Average dendrites (μm)	185 ± 13	149 ± 9	155 ± 10	0.080
Longest dendrite (μm)	183 ± 10	180 ± 11	172 ± 9	0.811

F

+GFP | +CRIPT | +pal-myc-CRIPT

Cell Parameter	+GFP (n=26)	+CRIPT (n=25)	+pal-myc-CRIPT (n=25)	*p*
Soma area (μm²)	235 ± 12Δ	221 ± 9	240 ± 10	0.406
1⁰ dendrites, #	6.0 ± 0.3	6.4 ± 0.3	6.7 ± 0.2	0.153
Branches, #	13.2 ± 0.8	13.1 ± 0.8	14.4 ± 0.8	0.154
∑length (μm)	1058 ± 58	1022 ± 44	1142 ± 62	0.294
Average dendrites (μm)	194 ± 17	165 ± 11	173 ± 9	0.403
Longest dendrite (μm)	187 ± 10	180 ± 11	193 ± 10	0.424

Figure 6

+GFP | +SAP97 +scrambled miRNA | +SAP97 +CRIPT miRNA

Cell Parameter	+GFP (n = 26)	+SAP97 +scrambled miRNA (n = 25)	+SAP97 +CRIPT miRNA (n = 25)	*p*
Soma area (μm²)	278 ± 10$^{\Delta}$	285 ± 17	257 ± 10	0.155
1⁰ dendrites, #	5.1 ± 0.3	5.0 ± 0.2	4.8 ± 0.2	0.530
Branches, #	10.0 ± 0.7	13.3 ± 1.1*	10.1 ± 0.6†	0.016
∑length (μm)	1037 ± 47	1292 ± 87*	1009 ± 48†	0.014
Average dendrites (μm)	217 ± 15	262 ± 18	219 ± 13	0.170
Longest dendrite (μm)	230 ± 11	251 ± 12	229 ± 11	0.310

Figure 7

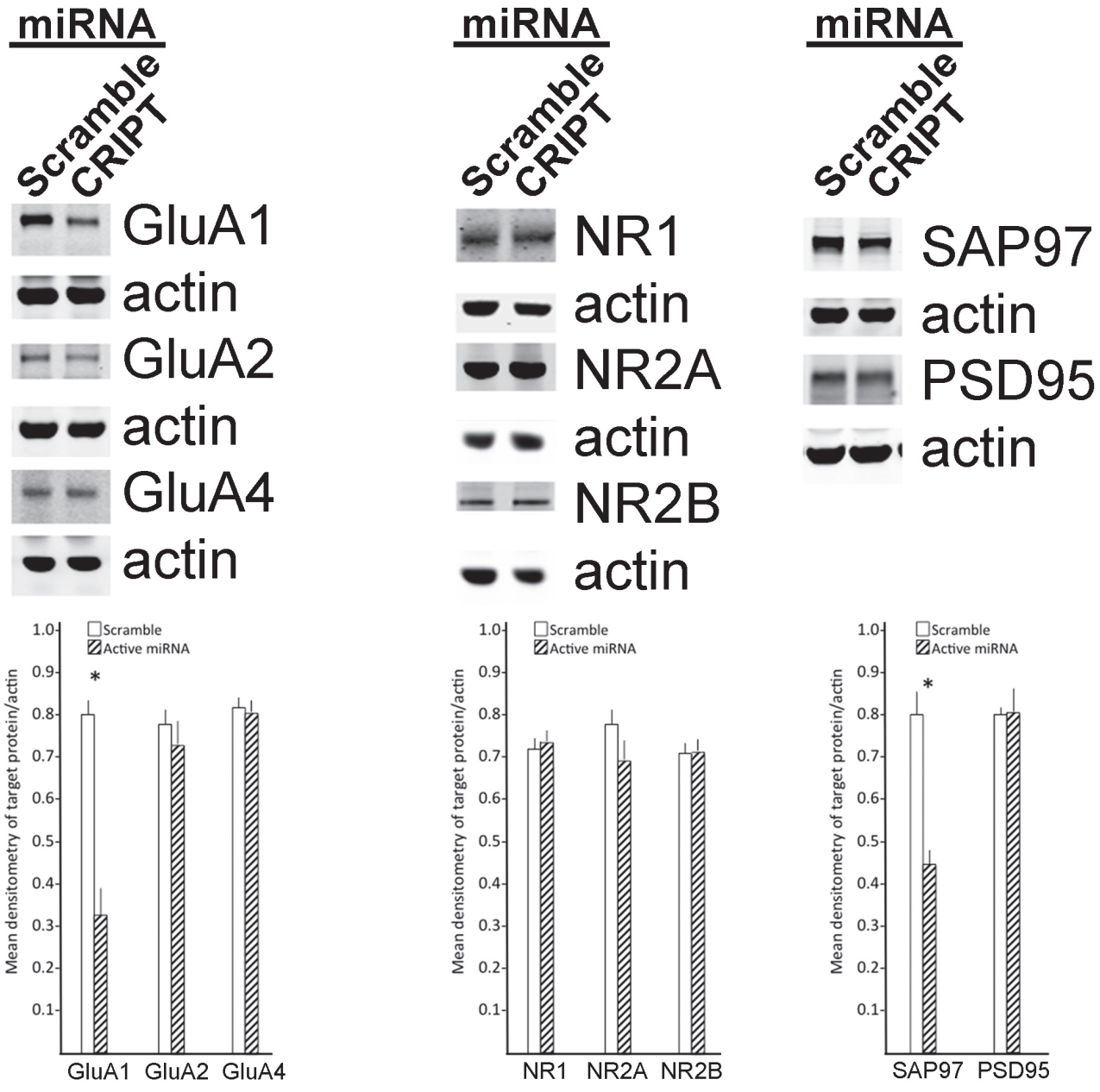

Figure 8